

FY2023 (2023.4-2024.3) NSEC Annual Report



Nuclear Science and Engineering Center
Nuclear Science Research Institute
Japan Atomic Energy Agency

October 2024

This report is issued by Japan Atomic Energy Agency.

Inquiries about availability and/or copyright of this report should be addressed to the Research Co-ordination and Promotion Office of the Nuclear Science and Engineering Center, Japan Atomic Energy Agency.

2-4 Shirakata, Tokai-mura, Naka-gun, Ibaraki-ken 319-1195 Japan.

E-mail: nsed-web@jaea.go.jp

© Japan Atomic Energy Agency, 2024

Table of Contents

Preface	1
R&D Highlights	2
Group Activities	9
Organization of NSEC	10
Nuclear Science and Reactor Engineering Division	11
Nuclear Data Center	
Research Group for Nuclear Sensing	
Research Group for Reactor Physics and Thermal-Hydraulics Technology	
Research Group for Nuclear Transmutation System	
Fuels and Materials Engineering Division	15
Research Group for Corrosion Resistant Materials	
Research Group for Radiation Materials Engineering	
Research Group for High Temperature Science on Fuel Materials	
Research Group for Nuclear Fuel Cycle Science	
Chemistry, Environment, and Radiation Division	19
Research Group for Environmental Science	
Research Group for Radiation Transport Analysis	
Research Group for Nuclear Chemistry	
Publication List	22

Preface

TSUJIMOTO Kazufumi

Director General, Nuclear Science and Engineering Center



The Nuclear Science and Engineering Center (NSEC) of the Japan Atomic Energy Agency (JAEA) aims to conduct research and development to advance the science and technology that supports the use of nuclear energy and radiation. This annual report provides research highlights and an overview of the research groups' activities in the NSEC for Fiscal Year 2023. We hope this annual report will increase your understanding of the NSEC.

The use of nuclear energy and radiation is supported by the underlying basic science and various technologies that link science and engineering. As such, we conduct fundamental research to elucidate various phenomena involving atomic nuclei, radiation, and radioactive materials using our innovative techniques for measurement and analysis. Based on modeling of the observed phenomena, we develop computer simulation codes and databases for predicting the behavior of energetic particles, heat and fluid in a reactor core, performance of nuclear fuel and reactor structural materials, properties and functions of radioactive materials related to their physical and chemical states, migration behavior of radionuclides in the environment, and the effects of radiation on the human body.

It is our responsibility to provide the results of our research and development activities to society in ways that are transparent and have high quality and impact. We have been disseminating our innovative technologies for resolving challenges in various fields, such as industry, environment, and medicine. The NSEC is a key research center for supporting the nuclear energy infrastructure through our nuclear science and engineering research. We strive to become a leading center for research collaboration, using our fundamental research and development capabilities to contribute to advances in science and technology.

We seek your understanding, support, and encouragement in our research and development activities.

September 2024

FY2023 NSEC R&D Highlights

The following 6 highlights are selected among various outcomes of the R&D activities accomplished by the NSEC's 3 divisions in FY2023.

✓ **Nuclear Science and Reactor Engineering Division:**

- ✧ *"Study on Atomization of a Wall-impinging Jet"*
- ✧ *"²⁴¹Am Neutron Capture Cross-section Measurement Using the NaI(Tl) Spectrometer Installed on the Accurate Neutron-nucleus Reaction Measurement Instrument Beamline of the Japan Proton Accelerator Research Complex"*

✓ **Fuels and Materials Engineering Division:**

- ✧ *"Estimating the Corrosion Rate of Stainless Steel in Nitric Acid Media during Concentration Operations"*
- ✧ *"Loss of the Protective Function of Cr-coated Zry Claddings in Accident Tolerant Fuel Applications"*

✓ **Chemistry, Environment, and Radiation Division:**

- ✧ *"Methodology for Rapid and Low-cost Estimation of Terrestrial Soft-error Rate"*
- ✧ *"Visualizing the Accurate Distribution of Trace Uranium in Environmental Samples Using Superconducting Technology"*

Study on Atomization of a Wall-impinging Jet

HORIGUCHI Naoki

Research Group for Reactor Physics and Thermal-Hydraulics Technology

Atomization is relevant to various scenarios in the nuclear field, such as the cooling of molten materials during severe accidents or the boiling transition in annular dispersed flows during the steady operation of a boiling water reactor. We studied the atomization of a wall-impinging jet in a shallow pool through numerical simulations¹⁾.

In a severe accident, jet atomization may occur, allowing molten fuel material to enter a shallow water pool, impinge on the floor, and spread three dimensionally. Atomization is critical in generating numerous droplets and enhancing the cooling of the molten fuel material jet, potentially influencing the progression of an accident. However, conducting full-scale tests to investigate jet atomization in detail is challenging. To address this, we simplified the molten fuel material jet as an immiscible jet in a liquid-liquid system and investigated its atomization using the following steps: 1) detailed numerical simulation with TPFIT²⁾, 2) validation of the overall behavior by comparing the numerical results with experimental data³⁾, 3) investigation of droplet formation as the elemental behavior of atomization, 4) development of a theoretical formulation for droplet formation, and 5) comparison of estimated values using the theoretical formulation.

In the following description, we present the results of numerical simulations based on steps 1)–3). Figure 1 illustrates the spreading behavior of a wall-impinging jet with atomization using a silicon oil and glycerin aqueous solution. Our results confirmed that the numerical simulations successfully reproduced the experimental results, including the circular spreading and atomization of the jet. Next, we focused on droplet formation and examined the detailed flow field information provided by the simulations. Figure 2 depicts the simulated droplet image, with velocity and pressure fields immediately after formation from an interfacial wave on a liquid film. We identified representative droplet formation patterns that vary depending on the jet's regions. Moreover, we developed a theoretical formulation based on interfacial instabilities and force balances related to droplet formation, confirming that the numerical data fit well with the values estimated from the formulation. These findings clarify the atomization mechanisms of the jet. This research is expected to contribute to the fundamental understanding of jet atomization and serve as a valuable reference for

simulating various scenarios in the nuclear field.

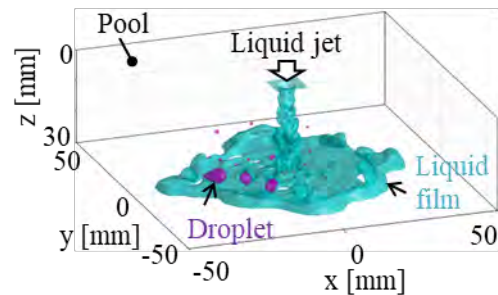


Fig. 1 Spreading behavior of a wall-impinging jet¹⁾

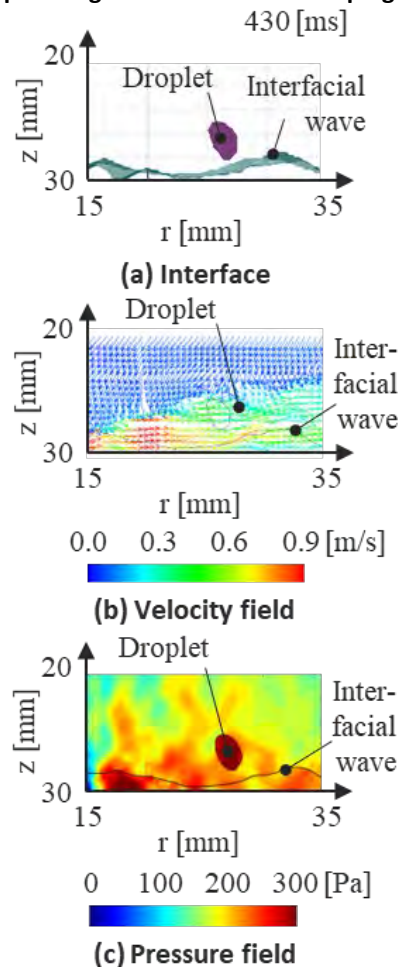


Fig.2 Flow fields immediately after droplet formation (430 ms after the start of impingement)¹⁾

References

- 1) N. Horiguchi, et al., *Phys. Fluids*. 35, 073309 (2023).
- 2) H. Yoshida, et al., *Trans. At. Energy Soc. Jpn.* 3(3), 233 (2004) (in Japanese).
- 3) S. Yamamura, et al., *Phys. Fluids*. 34, 082110 (2022).

²⁴¹Am Neutron Capture Cross-section Measurement Using the NaI(Tl) Spectrometer Installed on the Accurate Neutron-nucleus Reaction Measurement Instrument Beamline of the Japan Proton Accelerator Research Complex

ROVIRA Gerard¹, KIMURA Atsushi¹, NAKAMURA Shoji¹, ENDO Shunsuke¹, IWAMOTO Osamu¹, IWAMOTO Nobuyuki¹, KATABUCHI Tatsuya², KODAMA Yu², NAKANO Hideto², SATO Yaoki²

1 Nuclear Data Center

2 Laboratory for Zero-Carbon Energy, Institute of Integrated Research, Institute of Science Tokyo

Some advanced nuclear reactor systems aim to include minor actinides (MAs) in their core configuration. One such facility is an accelerator-driven system (ADS), which seeks to reduce the amount of MAs through nuclear transmutation. In some ADS designs, the core contains more than 50% MAs, with 20% of these MAs being ²⁴¹Am¹. However, to develop such facilities, several studies have emphasized the need for more accurate nuclear data on neutron-induced reactions, particularly the neutron capture cross-sections of ²⁴¹Am, given that it substantially contributes to the ADS criticality uncertainty. Despite extensive evaluations, previous experimental data still exhibit discrepancies exceeding 10% below 10 eV, where the cross-section is large, and uncertainties of up to 45% in the kiloelectron-volt region

The present experiments were conducted at the Accurate Neutron–Nucleus Reaction Measurement Instrument (ANNRI) beamline of the Materials and Life Science Experimental Facility at the Japan Proton Accelerator Research Complex². To improve accuracy, a fast NaI(Tl) spectrometer was used with a small sample containing 7.47 ± 0.10 mg of ²⁴¹Am packed in a 10-mm-diameter pellet with 46 mg of Y₂O₃ as a binder in an Al casing. This setup was aimed at suppressing the effects of detector deadtime and self-shielding, particularly at lower energies where the cross-section is large.

The neutron capture cross-section of ²⁴¹Am was measured from 10 meV to approximately 500 keV. Figure 1 compares the obtained results with the data contained in evaluated nuclear data libraries.

At thermal energy, the neutron capture cross-section was measured to be 708 ± 22 b, agreeing with the previous measurements conducted at the ANNRI by Terada et al.³, as well as the NEA WPEC evaluation⁴, and validating the evaluated data in JENDL-5⁵. In the resolved resonance region, resonance parameters up to 58 eV were derived through a resonance shape analysis, providing more accurate results in the region below 10 eV owing to reduced deadtime and self-shielding effects. Notably, the current study demonstrates reductions of 9% and 6% in the average area of resonances compared to the results of the latest analyses conducted by Terada et al.³ and Mendoza et al.⁶, respectively. In the resonance region over 100 eV, our results validate the current evaluated nuclear data; however, in the continuous region up to 10 keV, these results present slightly higher values compared to those included in the evaluated nuclear data libraries while reducing uncertainties in the cross-section. This implies that the evaluated nuclear data in the 700 eV–10 keV range must be improved based on the present results. Finally, above 10 keV, the present results align with both evaluated and experimental data while providing lower total uncertainties within 10%–20%

References

- 1) H. Iwamoto, et al., *J. Nucl. Sci. Technol.* 50, 856 (2013).
- 2) G. Rovira, et al., *J. Nucl. Sci. Technol.* 61, 459 (2024).
- 3) K. Terada, et al., *J. Nucl. Sci. Technol.* 55, 1198 (2018).
- 4) NEA WPEC SG 41, *Nuclear Science NEA/NSC/R(2020)2*.
- 5) O. Iwamoto, et al., *J. Nucl. Sci. Technol.* 60, 1 (2023).
- 6) E. Mendoza, et al., *Phys. Rev. C* 97, 1 (2018).

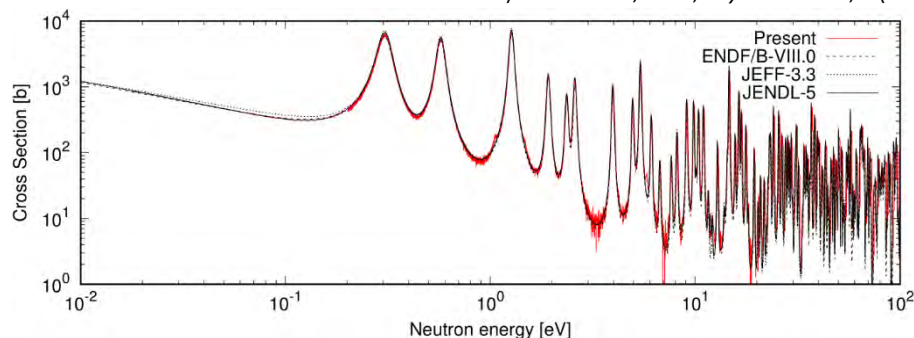


Fig. 1 Present ²⁴¹Am neutron capture cross section results (red) compared to the JENDL-5, ENDF/B-VIII.0 and JEFF3.3 evaluated nuclear data libraries

Estimating the Corrosion Rate of Stainless Steel in Nitric Acid Media during Concentration Operations

IRISAWA Eriko

Research Group for Corrosion Resistant Materials

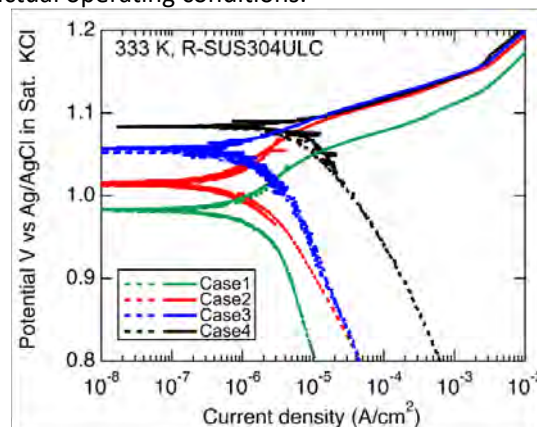
In the reprocessing solution used during the PUREX process, metal ions derived from spent fuels act as oxidants, leading to severe corrosion of stainless steel (SS) components. To address this issue, ultralow-carbon SS, R-SUS304ULC, was developed and is used at the Rokkasho Reprocessing Plant. Moreover, the decompression evaporation method is employed to minimize corrosion by lowering the operational temperature. Despite these efforts, severe corrosion caused a leakage incident in 2010, highlighting the need for improved corrosion evaluation methods and more accurate lifespan predictions for used materials¹⁾. The effects of changes in solution composition and boiling during actual high-level liquid waste concentration operations on SS corrosion were electrochemically clarified, leading to the development of an evaluation method for the assessment corrosion based on actual operating conditions.

This study simulated the corrosion on the inner surface of the highly active liquid waste concentrator (HALWC), made of R-SUS304ULC, during concentration operations. The effects of varying concentrations of HNO₃, metal ions in solution, and heating conditions on the corrosion rate were examined using the corrosion rates obtained from immersion tests and polarization curves from electrochemical measurements. The experiments covered four operational conditions: Case 1 at the start of concentration, Case 2 with higher HNO₃ concentration, Case 3 with decompression boiling at the same temperature, and Case 4 with metal ion concentrations similar to the final concentrations of concentrated liquid waste.

The study clarified the following factors that increase the corrosion rate:

1. Increasing the HNO₃ concentration affects anodic and cathodic reactions (Fig. 1²⁾) leading to a higher corrosion rate (Case 1 → Case 2).
2. Depressurized boiling increases the corrosion rate by raising the redox potential of the solution (Fig. 1²⁾, Case 2 → Case 3).
3. Metal ions such as ruthenium, vanadium, and cerium are oxidized to higher valence states by HNO₃, which cause the rising of the corrosion potential of the SS and the increasing the corrosion rate (Fig. 2²⁾).

By considering three parameters—acid concentration, metal ions, and solution boiling—corrosion predictions can be made, correlating with actual operating conditions.



Case1→Case2: Increasing concentration of HNO₃ from 3 to 8 mol/L (Same concentration of metal ions)
Case2→Case3: Heating with depressurize boiling (Same concentration of HNO₃ and metal ions)
Case3→Case4: Increasing concentration of metal ions by 5 times (With depressurize boiling, and same concentration of HNO₃)

Fig. 1 Polarization curves of R-SUS304ULC at 333 K under the simulated operating conditions of the HALWC²⁾

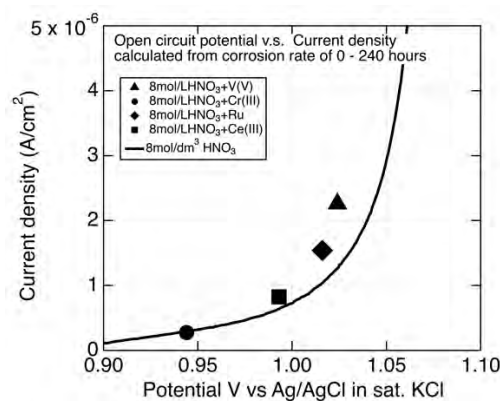


Fig. 2 Open circuit potential (OCP) versus corrosion rates in a solution containing V, Ru, Cr(III), and Ce. Effect of V, Ru, and Ce addition on the OCP and corrosion rate²⁾.

References

- 1) Revised report by Japan Nuclear Fuel Limited (2011), <https://www.jnfl.co.jp/press/pressj2010/pr110119-1.html> (accessed 2023-07-04) (in Japanese).
- 2) E. Irisawa, C. Kato, *J. Nucl. Mater.* 591, 154914 (2024).

Loss of the Protective Function of Cr-coated Zry Claddings in Accident Tolerant Fuel Applications

MOHAMAD Afifa

Research Group for High Temperature Science on Fuel Materials

Cr-coated zirconium alloy (Zry) claddings, FeCrAl, and SiC are well-known cladding candidates for accident tolerant fuel (ATF) owing to their superior oxidation resistance compared to that of normal Zry claddings. To utilize these materials in light water reactors, screening under normal operation (NO) and accident conditions is necessary. For Cr-coated materials, numerous studies focusing on integral or small-scale tests simulating NO and accident conditions have been reported. However, several questions remain regarding the oxidation behavior of Cr-coated materials near the Cr–Zr eutectic temperature of 1332°C, particularly under severe accident scenarios. Our study examined the oxidation behavior of Cr-coated Zry claddings at high temperatures through oxidation tests, primarily above the eutectic temperature.

Figure 1 illustrates the transition of the protective Cr coating to a nonprotective one on Zry claddings. Protection loss is caused by Zr migrating into the Cr layer and precipitating along Cr grain boundaries (GBs). Oxygen preferentially reacts with Zr at these GBs to form ZrO_2 , creating a short path for O diffusion, which subsequently reacts with the interlayer and substrate regions. Consequently, ZrO_2 layers form in the substrate regions, indicating that the Cr coating no longer protects the Zry cladding. This phenomenon is confirmed in high-temperature tests at 1200°C for at least up to 5 min.

Further, we observed a transition in the intermetallic phase, $Zr(Cr,Fe)_2$, within the substrate regions of Zry. Initially, the intermetallic phase formed owing to Cr diffusion into the coating at high temperatures. Below 1200°C ($T < T_{\text{eutectic}}$), the intermetallic phase formed as a Widmanstätten structure (Fig. 2(a)). Near the eutectic temperature ($T \approx T_{\text{eutectic}}$), it appeared as a globular structure (Fig. 2(b)). Above 1400°C ($T > T_{\text{eutectic}}$), a dendritic structure (Fig. 2(c)) was observed.

This research investigated the behaviors of Cr-coated Zry claddings under high-temperature steam oxidation, defining the transition from a “protective coating” to a “nonprotective coating.” Moreover, the study clarified the intermetallic phase transition below and above the Cr–Zr eutectic temperature.

This research was a collaboration between JAEA and Mitsubishi Heavy Industries, Ltd., contributing to the development of ATF in Japan.

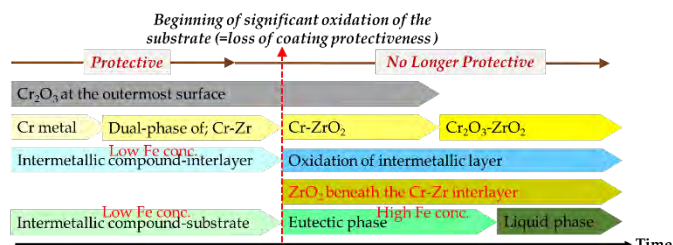


Fig. 1 Illustration of major phenomena observed during the transition of the “protective coating” to a “nonprotective coating”^{1,2)}

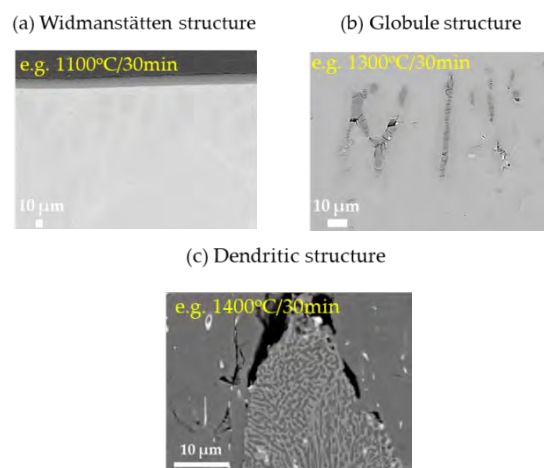


Fig. 2 Appearance of the $Zr(Cr,Fe)_2$ intermetallic phase at 1100°C, 1300°C, and 1400°C as (a) a Widmanstätten structure, (b) globule structure, and (c) dendritic structure^{1,2)}

References

- 1) A. Mohamad, et al., *Corrosion Science*, 224, 11540 (2023).
- 2) A. Mohamad, et al., *Proc. 28th International QUENCH Workshop* (2023).

Methodology for Rapid and Low-cost Estimation of Terrestrial Soft-error Rate

ABE Shin-ichiro

Research Group for Radiation Transport Analysis

The single event upset (SEU) phenomena induced by terrestrial neutrons are the primary causes of nondestructive faults (soft errors) in microelectronic devices on the ground. Evaluations of the terrestrial soft-error rate (SER), SER_{GND} , are essential for ensuring device reliability. Some spallation neutron fields with energy spectra similar to those of terrestrial neutrons have been utilized to estimate SER_{GND} . However, such special fields are limited and fail to meet global testing demands. Another evaluation method uses the four-parameter Weibull function to fit the SEU cross-section, σ_{SEU} , measured by (quasi-)mono-energetic neutron and/or proton sources. However, the Weibull function method requires at least four experimental datapoints with different energies to determine the fitting parameters. If SER_{GND} can be evaluated using one-time neutron irradiation and various types of neutron sources (i.e., sources with energy spectra not similar to terrestrial neutron), we can address beam time shortages and reduce SER_{GND} estimation cost.

We developed a new methodology to estimate SER_{GND} based on simulations and one-time neutron irradiation testing¹. Figure 1 illustrates the procedure adopted to derive SER_{GND} . The SEU cross-section, $\sigma_{SEU}(E_n, Q_{fit})$, as a function of the incident neutron energy, E_n , and the critical charge, Q_{fit} , are computed under varying E_n . Q_{fit} is treated as the only adjustable parameter and is determined using a single measured data. After Q_{fit} is determined, SER_{GND} is calculated by

$$SER_{GND} = \int \sigma(E_n, Q_{fit}) \phi_{GND}(E_n) dE_n \quad (1)$$

where $\phi_{GND}(E_n)$ represents the energy spectrum of terrestrial neutrons at the ground level.

Figure 2 shows the SER_{GND} estimated via our method using a single measured data. For comparison, the SER_{GND} values estimated using the step function method are also included as another conventional method to estimate SER_{GND} by one-time neutron irradiation. As a reference, SER_{GND} estimated by the Weibull function method is shown in Fig. 2. Our method provides reasonable SER_{GND} data regardless of the single measured data used to determine Q_{fit} , while some SER_{GND} estimates obtained using the step function method substantially differ from those obtained using the Weibull function method. This result validates the proposed SER_{GND} estimation method. Moreover, our method is quicker and less costly than the

Weibull function method because it requires only one-time neutron irradiation testing. Thus, we anticipate that our method will also be applicable to the estimation of SER_{GND} for other semiconductor devices, and experimental validation in this regard is ongoing.

This work was supported by the Japan Science and Technology Agency (JST) through the Program on Open Innovation Platform with Enterprises, Research Institute and Academia (OPERA), under Grant JPMJOP1721.

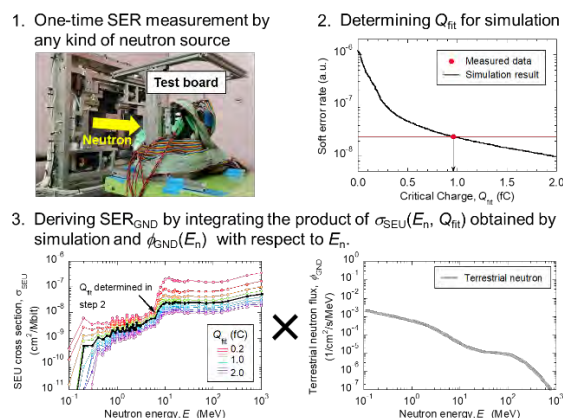


Fig. 1 Procedure to derive SER_{GND}

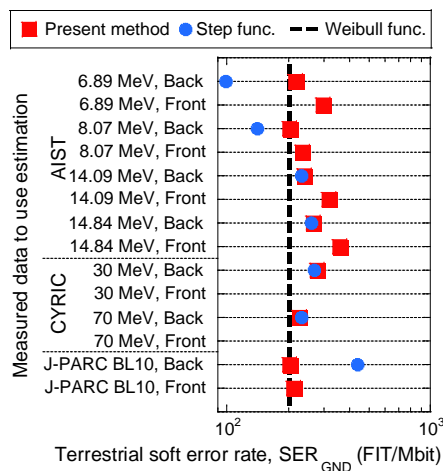


Fig. 2 SER_{GND} estimated by our method, step function method and Weibull function method

Reference

1) S. Abe, et al., *IEEE Trans. Nucl. Sci.* 70(8), 1652 (2023).

Visualizing the Accurate Distribution of Trace Uranium in Environmental Samples Using Superconducting Technology

YOMOGIDA Takumi¹, HASHIMOTO Tadashi², FUKUSHIMA Shigeru³, KITATSUJI Yoshihiro¹

1 Research Group for Nuclear Chemistry

2 Advanced Science Research Center

3 Ningyo-toge Environmental Engineering Center

U is widely used as fuel for nuclear power generation worldwide. Understanding the migration behavior of U in the subsurface environment is crucial for nuclear waste disposal. Micro-X-ray fluorescence–X-ray absorption near edge structure (μ -XRF–XANES) analysis is a powerful method for U distribution and chemical species analysis. However, the energy resolution of commonly used semiconductor detectors is insufficient owing to the presence of various elements in environmental samples. Fluorescence X-rays from trace amounts of U can interfere with the fluorescence X-rays of other abundant elements (e.g., Rb) in the earth’s crust, making it difficult to accurately determine the distribution and chemical species of U.

In this study, we used a superconducting transition-edge sensor (TES), which offers high energy resolution and high detection efficiency¹. Figure 1 illustrates the μ -XRF spectra of a biotite sample, including the Rb $K\alpha$ and U $L\alpha_1$ lines recorded by a conventional silicon drift detector (SDD) and the TES. In the μ -XRF spectrum obtained using the SDD, the U $L\alpha_1$ line at 13.615 keV is obscured by the Rb $K\alpha$ line at 13.376 keV (Fig. 1(a)). Conversely, the U $L\alpha_1$ line is clearly observed when using the TES because of its high energy resolution (Fig. 1(b)). Figure 2 presents a comparison of the SDD and TES mapping analysis results of the biotite sample. The conventional SDD could detect only the fluorescence X-rays of the Rb $K\alpha$ line, which is abundant in biotite, and could not accurately detect trace amounts of U (Fig. 2(a)). In contrast, TES mapping results highlighted differences in the distributions of Rb and U (Fig. 2(b)). These results demonstrate that accurate analysis of trace amounts of U is possible using the TES; such analyses are difficult to achieve using conventional semiconductor detectors. Moreover, the simultaneous μ -XANES measurements successfully analyzed the chemical state of U in biotite, revealing partial reduction of U, thereby indicating reduced mobility.

Although the aforementioned experiment focused on U and Rb in environmental samples, the TES was confirmed to exhibit high energy resolution up to 17 keV. This suggests that the TES

can be applied to analyze other elements with fluorescence X-rays in this energy range, with promising applications for various environmental samples in the future.

This work was supported by the Grants-in-Aid for Scientific Research (KAKENHI) from the MEXT (grant nos. 18H05458, and 21H00162) and JSPS (grant nos. 19H01145, 19H01960, 19K15606, 19K21893, 19K23432, 20K20527, 20K15238, 20K14524, 21H03585, 21H05443, 21K18649, 21K18917, 22F21313, 22H00166, and 22K18277). This study was performed with the approval of JASRI/SPring-8 (proposal nos. 2022A0174, 2022A0180, 2021A1610, 2019A1523, 2019B1498, and 2020A0174) and the Photon Factory (2022G126, 2020G670, 2020G081, and 2018S1-001).

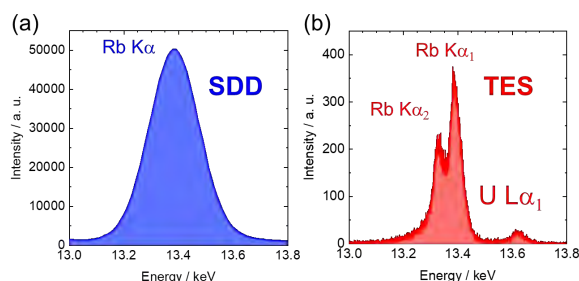


Fig. 1 μ -XRF spectra of the biotite sample recorded using (a) SDD and (b) TES at an excitation energy of 17.2 keV

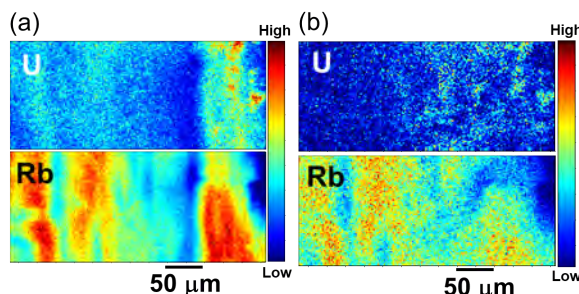


Fig. 2 μ -XRF imaging of the biotite sample. μ -XRF U and Rb map images recorded using (a) SDD and (b) TES

Reference

1) T. Yomogida, et al., *Analyst* 149, 2932 (2024).

FY2023 NSEC Group Activities

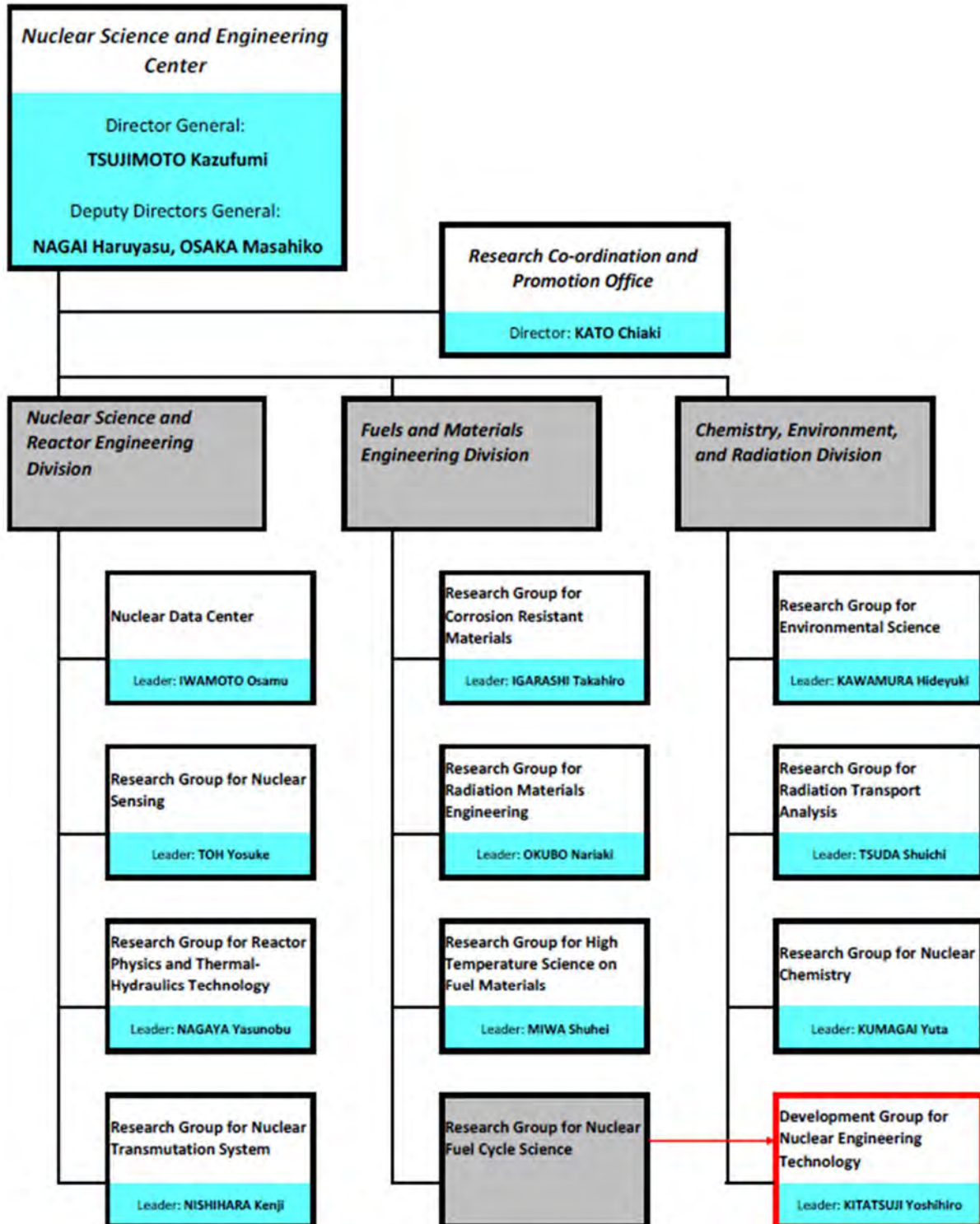
The NSEC of JAEA consists of 11 Groups.

Since April 2024, the NSEC has been re-organized as follows

- ✓ *3 Divisions have been abolished.*
- ✓ *“**Research Group for Nuclear Fuel Cycle Science**” has been renamed “**Development Group for Nuclear Engineering Technology.**”*

Organization of NSEC

(as of October 2024)



URL: https://nsec.jaea.go.jp/organization/en_index.html

Nuclear Data Center

The Nuclear Data Center provides reliable nuclear data for various devices, such as nuclear reactors and accelerators, and technologies, such as medical radiation. Based on collaboration with nuclear data researchers and organizations worldwide, our research focuses on theories, measurements, and evaluations related to nuclear reactions and structures. The evaluated nuclear data are compiled into the Japanese Evaluated Nuclear Data Library (JENDL), which is accessible through our website (<http://www.ndc.jaea.go.jp>).

Thermal Neutron Capture Cross-section Measurements Using Research Reactors

Research reactors create well-characterized neutron irradiation fields that enable accurate measurements of neutron capture cross-sections using activation methods. Neutron capture reactions producing long-lived radioisotopes (RIs) are crucial for evaluating activities in nuclear facilities. However, for RIs with excessively long half-lives, traditional activation methods, which rely on decay radiation assessments, may be ineffective owing to their weak radioactivity levels. To address this, we employed mass spectrometry to determine the capture cross-section of ^{204}Pb , which produces ^{205}Pb (half-life = 1.73 million years), using samples irradiated at the Japan Research Reactor-3. The measured ratio of ^{205}Pb to ^{204}Pb was 8.4×10^{-5} with 4% uncertainty, corresponding to a thermal neutron capture cross-section of 0.53 b¹⁾. This result suggests a possible overestimation in the JENDL-5 evaluation data, which report a value of 0.70 b for this cross-section. Furthermore, the Kyoto University Research Reactor (KUR) was employed to measure the cross-section of ^{93}Nb . Samples irradiated at the KUR were analyzed using gamma-ray and mass spectroscopy techniques, yielding a thermal neutron capture cross-section of 1.11 b with 4% uncertainty and a half-life of 20 thousand years with 8% uncertainty²⁾. These findings are consistent with the current evaluated data in JENDL-5 within the experimental uncertainties.

Time-of-flight Measurements for Neutron Cross Sections

The Accurate Neutron–Nucleus Reaction Measurement Instrument (ANNRI), installed at the Materials and Life Science Experimental Facility of the Japan Proton Accelerator Research Complex, is among the most attractive instruments for nuclear

measurements using the time-of-flight method owing to its high neutron flux. We measured the neutron total and capture cross-sections for Gd, Ta, and La isotopes using the ANNRI. Despite the importance of Gd cross-sections, the values of which are considerably high for thermal neutrons, previous experimental data are scattered. Furthermore, the latest measurement data released in JENDL-4.0 indicate lower values for Gd cross-sections, adding to the previous confusion. However, our recent measurements conducted using the ANNRI³⁾ support higher Gd cross-sections, and the evaluation data in JENDL-5 reflect these updated results.

Feasibility Study of Fast Neutron Source with Deuteron by JENDL-5

We investigated deuteron-induced reactions on Be to assess their potential for use in compact fast-neutron sources⁴⁾. JENDL-5 includes a deuteron sublibrary containing neutron emission spectral data obtained from deuteron-induced reactions on Be. We utilized these JENDL-5 data to simulate neutron sources using the particle transport code Particle and Heavy Ion Transport code System. The reliability of the deuteron nuclear data provided by JENDL-5 was confirmed by comparing the calculated results with experimental data on high target-neutron yields obtained from deuteron. Furthermore, the results of neutron source simulations using a deuteron beam were compared with those obtained using a proton beam and a Li target, which has been considered a potential neutron source candidate. The results revealed that a deuteron beam in an energy range of 1.5–2.5 MeV could serve as a viable neutron source, provided that the shielding thickness is increased by approximately 1.5 times that required for a 2.5 MeV proton beam, which carries higher energy.

References

- 1) S. Nakamura, et al., *J. Nucl. Sci. Technol.* 60(9), 1133 (2023).
- 2) S. Nakamura, et al., *J. Nucl. Sci. Technol.* 60(1), 1361 (2023).
- 3) A. Kimura, et al., *J. Nucl. Sci. Technol.* 60(6), 678 (2023).
- 4) S. Nakayama, *J. Nucl. Sci. Technol.* 60(12), 1447 (2023).



Contact (Group Leader):

IWAMOTO Osamu

iwamoto.osamu@jaea.go.jp

Research Group for Nuclear Sensing

In nuclear security, nondestructive assay (NDA) techniques are indispensable for nuclear material (NM) accountancy. In particular, neutron-based NDA techniques are crucial owing to the high penetrating power of neutrons and their ability to induce nuclear fission reactions within nuclear fuel materials. We are conducting research and development on neutron-based NDA techniques to facilitate implementation of the NM accountancy system for highly radioactive NMs, which are difficult to analyze using conventional methods. The following description outlines some of our activities in FY2023.

Development of Active-N

NM accountancy systems must accurately measure the amount of NMs. Differential die-away analysis (DDA) is highly effective for this purpose as it rapidly and precisely quantifies the total fissile NM content by detecting induced fission neutrons. Although this method can measure the total NM quantity (Pu effective mass), it is currently unable to determine individual isotope contents. Neutron resonance transmission analysis (NRTA) is a powerful method that can be used to accurately determine the isotopic ratios of NMs by detecting neutrons transmitted through a sample. Although NRTA provides highly precise results, conventional NRTA facilities typically require large-scale particle accelerators. Notably, the results of both the NRTA and DDA methods are considerably influenced by the presence of neutron poisons (e.g., ^{10}B and Gd) within their samples. Such poisons reduce the number of detectable neutrons through nuclear reactions. Prompt gamma-ray analysis (PGA) mitigates these effects by detecting the gamma rays emitted during reactions. To integrate these three complementary measurement methods—NRTA, DDA, and PGA—and adapt them for use in existing nuclear facilities, such as spent-fuel processing plants handling highly radioactive NMs, we developed a compact integrated NDA system called Active-N (Fig. 1)¹⁾.

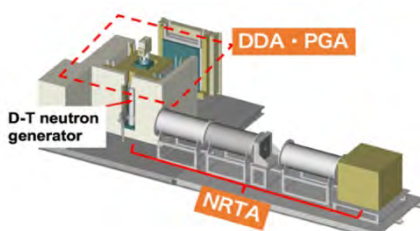


Fig. 1 Schematic view of Active-N

For size reduction, the system utilizes a D-T neutron

generator, emitting 14 MeV neutrons isotropically at a rate of up to $2 \times 10^9 \text{ s}^{-1}$, as the neutron source. This neutron source is shared across the three methods. The following sections describe the developments and achievements of the NRTA, DDA and PGA methods:

(1) NRTA The isotropically emitted neutrons lead to substantial neutron and gamma-ray background (BG) radiation, complicating NRTA measurements. To address this, a detector shield and collimators have been developed to minimize the number of neutrons reaching the detector without passing through the sample. Furthermore, a detector capable of eliminating >99% of BG signals through pulse shape discrimination has been incorporated. These advancements have enabled implementation of NRTA in Active-N to accurately determine the isotopic ratios of NMs.

(2) DDA To measure the amounts of highly radioactive NMs, the system is equipped with 60 ^{10}B neutron detectors, with 5-cm-thick Pb shields placed between the sample and detectors. The utilized materials are optimized to avoid interference with PGA measurements. Several test measurements have demonstrated that the system can detect as little as 20 mg of plutonium and effectively operates even in the presence of intense neutron BG radiation of up to $1.57 \times 10^7 \text{ s}^{-1}$ and gamma radiation of up to $4.43 \times 10^{10} \text{ s}^{-1}$.

(3) PGA In PGA measurements, both the sample and PGA detector are bombarded by the isotropically emitted neutrons. To shield the detectors and simultaneously reduce the emission of gamma rays from the $\text{H}(n,\gamma)$ reaction, LiF-mixed polyethylene shields have been utilized. Based on preliminary measurements, the materials employed in the integrated system have been selected to reduce gamma BG radiation, achieving a gamma counting rate as low as $3.9 \times 10^3 \text{ s}^{-1}$ ²⁾.

This research was funded by the Ministry of Education, Culture, Sports, Science and Technology for nuclear security promotion.

References

- 1) H. Tsuchiya, et al., *J. Nucl. Sci. Technol.* 60, 1301 (2023).
- 2) K. Furutaka, et al., *Nucl. Eng. Technol.* 55, 4002 (2023).



Contact (Group Leader):

TOH Yosuke

toh.yosuke@jaea.go.jp

Research Group for Reactor Physics and Thermal-Hydraulics Technology

Our group focuses on reactor physics and thermal hydraulics, with a mission to develop individual technologies and multiphysics simulation tools. Currently, we are focusing on the development of an advanced neutronics/thermal hydraulics coupling simulation system to enhance the safety of light water reactors (LWRs) and improve LWR designs.

JAMPAN

JAMPAN¹⁾ is a new multiphysics platform designed to accommodate coupling simulations, enabling advanced neutronics/thermal hydraulics coupling modeling. We conducted a null transient (time-dependent steady-state) simulation on the JAMPAN platform using the neutronics code MVP and the thermal hydraulics subchannel code NASCA^{2,3)}. Figure 1 illustrates the calculation geometry for 2 x 2 boiling-water-reactor fuel assemblies with varying burnup points. For detailed assembly information, refer to Reference 4. Figure 2 presents the calculated k-infinity value as a function of time. Notably, convergence for the coupling was achieved after several iterations. Furthermore, we successfully implemented flow-rate adjustments for multiple-assembly calculations.

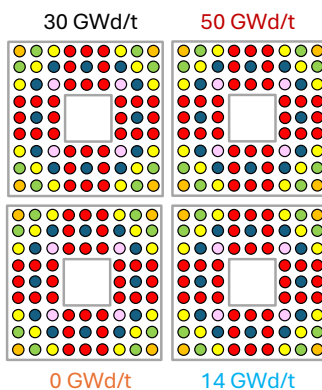


Fig. 1 Calculation geometry for 2 x 2 BWR fuel assemblies

AI-based Bubble Detection

Validating thermal hydraulics codes based on computational fluid dynamics is essential. To this end, we performed two-phase flow experiments and developed two-phase flow measurement techniques. Recently, we also introduced a new bubble detection technique based on deep learning⁵⁾. Figure 3 compares the bubble detection

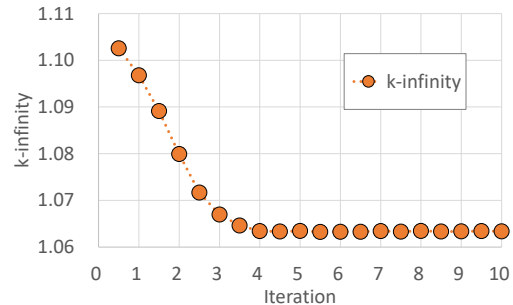


Fig. 2 Calculated k-infinity value as a function of iteration

accuracy of various methods. Notably, the new deep-learning-based method accurately detects bubbles that were previously misidentified by the existing method (which relies on contour extraction based on luminance value differences) (A and A' in the figure) and identifies new bubbles that were previously undetected (B and B' in the figure).

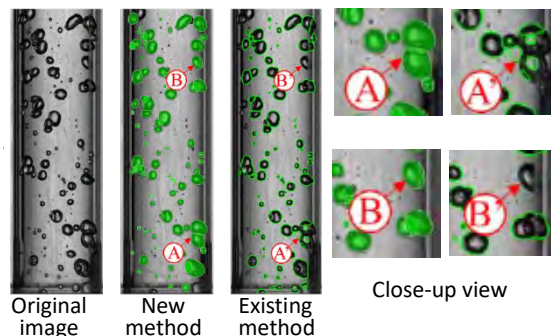


Fig. 3 Comparison of the detection images between the new and existing methods

References

- 1) T. Kamiya, et al., *Proc. ICONE29, ICONE29-91828* (2022).
- 2) K. Tada, et al., *Proc. Physor 2024* (2024).
- 3) K. Tada, et al., *2024 Annual Meeting of AESJ, 2L14* (2024) (in Japanese).
- 4) H. Okuno, et al., *JAERI-Research 2002-001* (2002).
- 5) S. Uesawa, et al., *J. Nucl. Sci. Technol.*, in press (2024), <https://doi.org/10.1080/00223131.2024.2348023>.



Contact (Group Leader):
 NAGAYA Yasunobu
 nagaya.yasunobu@jaea.go.jp

Research Group for Nuclear Transmutation System

The research group for nuclear transmutation system is developing an accelerator-driven system (ADS) tailored for the transmutation of minor actinides (MAs) into short-lived or stable nuclides. Unlike conventional reactors, which are fueled by uranium and Pu, the ADS is primarily fueled by MAs. To boost the reliability of the ADS design, previous experiments studying the interactions between MAs with neutrons within the reactor are being reanalyzed. Furthermore, research on the transmutation of light water reactor (LWR) mixed oxide (MOX) fuel is also underway, focusing on MOX fuel disposal methods and evaluations of the effects of transmutation.

MA Nuclear Data Measurement

In the early 1980s, several integral experiments were conducted in the Fast Critical Assembly to evaluate the fission and capture cross-sections of transuranic nuclides, including MAs. These experiments were performed using seven uranium-fueled assemblies (IX-1 – IX-7) whose neutron energy spectra were adjusted to vary from intermediate-neutron to fast-neutron spectra. Small sample reactivity worths (SRWs) of ^{237}Np , ^{238}Pu , ^{240}Pu , ^{241}Am , and ^{243}Am were determined. These SRWs were recently re-evaluated based on the updated knowledge of experimental conditions through detailed uncertainty analysis, and the most recent analysis methods, including the latest nuclear data library Japanese Evaluated Nuclear Data Library-5, were validated.

The results revealed that the analysis method accurately predicted the experimental SRWs of ^{237}Np across all assemblies (IX-1 – IX-7) (Fig. 1).

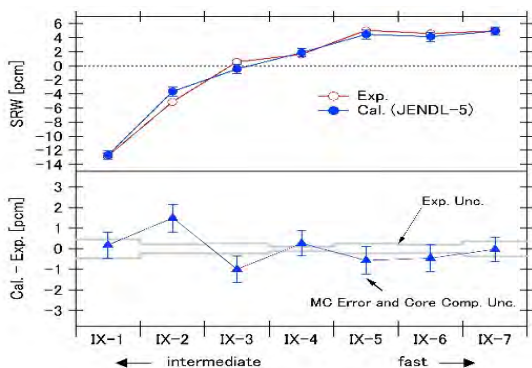


Fig. 1 Comparison between calculations and experiments of SRW of ^{237}Np ¹⁾

However, the results for ^{241}Am and ^{243}Am deviated from the corresponding experimental data, particularly for the fast-neutron spectra (IX-5–IX-7),

highlighting the need for further refinement of the nuclear data library. These adjustments must integrate the current results with previously measured fission rate ratios for these nuclides from the same experimental series.

Disposal of Spent MOX Fuel from LWR

In Japan, Pu is utilized as an MOX fuel for LWRs, with plans to reprocess the spent MOX fuel as fast reactor fuel in the future. However, preparing for the possibility that the spent MOX fuel may have to be directly disposed owing to policy changes is essential. Notably, given that spent MOX fuel generates substantially greater amounts of heat compared to spent UO_2 fuel owing to MAs, existing direct disposal concepts for spent UO_2 fuel are unsuitable because of the temperature criteria in the repository (<100°C). To address this, we investigated the effects of modifying four design parameters (cooling term, disposal depth, buffer thickness, and occupied area) on the temperature criteria of the disposal concepts. By extensively varying these parameters, we developed some new disposal concepts meeting the temperature limits, as shown in Table 1. The resulting temperature database has been implemented in the nuclear fuel cycle simulator NMB4.0, enabling mass balance analysis, including MOX fuel direct disposal.

Table 1 Comparison of the disposal concepts²⁾

	Cooling term [y]	Disposal depth [m]	Buffer thickness [m]	Occupied area [m ²]	Max. buffer temp. [°C]
UO_2	54	1,000	0.7	126	89
MOX	75	600	0.45	360	96

References

- 1) M. Fukushima, et.al, *J. Nucl. Sci. Technol.* 61(4), 478 (2024).
- 2) T. Abe, K. Nishihara, *J. Nucl. Sci. Technol.* 61(8), 1048 (2024).



Contact (Group Leader):
NISHIHARA Kenji
nishihara.kenji@jaea.go.jp

Research Group for Corrosion Resistant Materials

Our research group focuses on investigating the corrosion phenomena of metallic materials used in nuclear facilities. Corrosion can degrade reactor components, leading to hole and crack formation. Hence, we aim to understand various corrosion mechanisms to develop reliable corrosion prediction and prevention methods, thus improving the reliability and longevity of nuclear facilities.

Effect of Dissolved Oxygen on Corrosion Behavior at the Crevice Surface in High-temperature Water under Gamma-ray Irradiation

To evaluate the influence of dissolved oxygen concentration on water radiolysis within cracks formed by stress corrosion cracking under irradiation, we conducted immersion tests on stainless steel specimens with crevices, along with computer simulations of water radiolysis. Our results revealed Fe_2O_3 formation throughout the crevice region, irrespective of the dissolved oxygen concentration¹⁾ (Fig. 1). Furthermore, we observed that oxidant species generated through radiolysis within the cracks were consumed during oxide formation under irradiation. This suggests that the pH at the crack tip decreased owing to the hydrolysis of dissolved metallic elements.

Synergistic Effect of Aluminum Lactate and Sodium Molybdate on the Freshwater Corrosion of Carbon Steel under Irradiation

Previously, we proposed a novel corrosion inhibitor to protect the primary containment vessels at the Fukushima Daiichi Nuclear Power Station. Given the internal conditions of these vessels, the inhibitor is required to prevent carbon steel corrosion under irradiation. Furthermore, the concentration of this inhibitor must adhere to the effluent standards of Japan. The two components of the novel corrosion inhibitor, aluminum lactate and sodium molybdate, were found to be the most effective at concentrations of 0.75 (aluminum lactate) and 0.25 (sodium molybdate) mM. Furthermore, the inhibitor prevents the corrosion of carbon steel even under gamma irradiation of 200 Gy/h. We observed that the aluminum and molybdate formed a metal cation layer on the carbon steel with few defects and no iron. This layer suppressed both the cathodic oxygen reduction and anodic iron dissolving reactions²⁾ (Fig. 2).

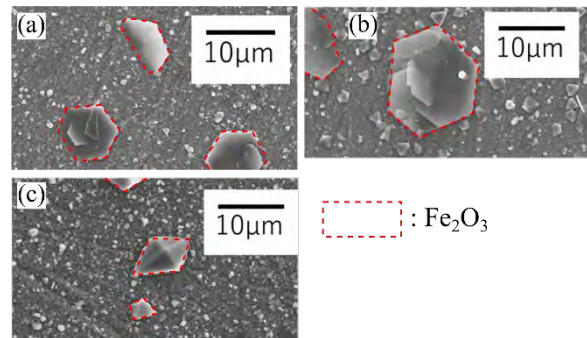


Fig. 1 Scanning electron microscopy images of the inner crevice surface of a test specimen under various dissolved oxygen (DO) concentrations: (a) DO < 0.005, (b) < 0.2, and (c) = 2 ppm

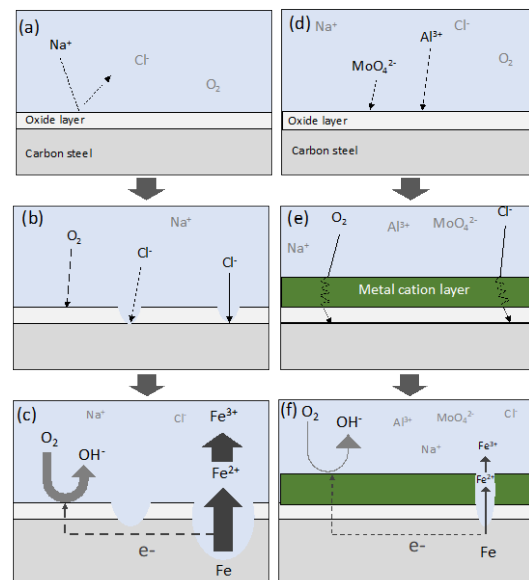
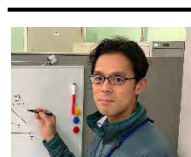


Fig. 2 Schematics of the corrosion behavior of carbon steel: (a)–(c) without the developed inhibitor and (d)–(f) with the developed inhibitor

References

- 1) T. Sato, et al., *Zairyo-to-Kankyo* 73(4), 102 (2023) (in Japanese).
- 2) K. Otani, et al., *Corrosion* 79(11), 1277 (2023).



Contact (Group Leader):
IGARASHI Takahiro
igarashi.takahiro@jaea.go.jp

Research Group for Radiation Materials Engineering

The mechanical properties of materials change as their microstructures evolve in the radiation environments of nuclear power systems such as light water reactors, future accelerator-driven systems, and advanced nuclear systems. To predict the property changes of nuclear materials, we examine their microstructural evolution through a combination of experimental and computational approaches. Notably, for obtaining better nuclear material candidates, fundamental and engineering research is crucial for elucidating the mechanisms underlying radiation-induced embrittlement¹⁾, radiation-induced damage in ceramics²⁾, and crevice corrosion, which is related to stress corrosion cracking (SCC)³⁾.

Ion Tracks and Nanohillocks Created in Natural Zirconia Irradiated with Swift Heavy Ions

Natural monoclinic zirconia (baddeleyite) was irradiated with 340 MeV Au ions, and the resulting irradiation-induced nanostructures (i.e., ion tracks and nanohillocks) were observed through transmission electron microscopy (TEM)²⁾. The TEM images revealed that the tracks appeared as strained regions that maintained their crystalline structure (Fig. 1). Most ion tracks exhibited rectangular cross-sections up to 10 nm in size, indicating anisotropic recrystallization of the molten region, reflecting the lattice structure of the material (Fig. 1). Furthermore, low-density track cores were observed at the centers of the ion tracks, attributed to the ejection of molten matter toward the surface. Comparing the ion tracks in synthetic zirconia nanoparticles with those in larger natural zirconia samples revealed that the interfaces between the strained tracks and the matrix were less distinct in the synthetic samples. These findings suggest that recrystallization was influenced by the dimensions of the irradiated samples.

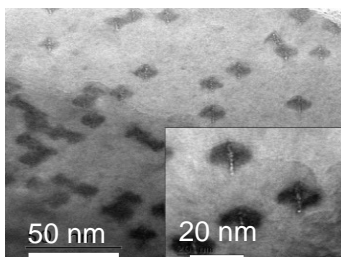


Fig. 1 TEM image of the ion tracks formed in natural zirconia irradiated with 340-MeV Au ions²⁾. The inset illustrates low-density cores with strain fields.

Time-lapse Observation of Crevice Corrosion in Grade 2205 Duplex Stainless Steel

To elucidate the mechanism underlying crevice corrosion, which can trigger SCC, a study was conducted to precisely visualize the spatial and temporal progression of crevice corrosion in grade 2205 duplex stainless steel using time-lapse imaging³⁾. A transparent polymethyl methacrylate washer and disk were coupled with the duplex stainless steel specimen to create an artificial crevice. The nucleation sites and corroding areas within the crevices were imaged in situ using a digital microscope setup. The results revealed that localized corrosion initiated near the edge of the washer, where the crevice gap was very narrow, creating active corrosion sites. The corrosion then propagated underneath the disk into regions with wider gaps, extending toward the crevice mouth (Fig. 2). This led to the development of distinct corrosion regions: areas where austenite (γ) selectively dissolved, a region where both austenite and ferrite dissolved, and a region where only ferrite (α) dissolved. This study demonstrated that the combination of an applied electrochemical potential with time-lapse imaging serves as a powerful tool for in situ corrosion analysis.

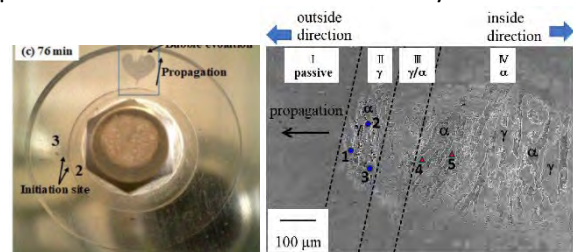


Fig. 2 Photograph of in situ crevice corrosion (left) and SEM image of the corroded area inside the crevice³⁾: (I) passive zone, (II) γ phase dissolution zone, (III) γ and α phase dissolution zone, and (IV) α phase dissolution zone (right)

References

- 1) S. Ukai, et al., *Mater. Charact.* 211, 113813 (2024).
- 2) N. Ishikawa, et al., *Materials* 17, 547 (2024).
- 3) S. Aoki, et al., *Materials* 16, 5300 (2023).



Contact (Group Leader):
OKUBO Nariaki
okubo.nariaki@jaea.go.jp

Research Group for High Temperature Science on Fuel Materials

We conduct research and development on advanced nuclear fuels, fuel debris characteristics, and fission product (FP) behavior during severe accidents (SAs) to support the sustainable development of nuclear energy. Our research involves both cold- and hot-material experiments, utilizing various high-temperature heating devices, analytical instruments, and property analysis tools. We also integrate computational science to complement our experimental findings, applying first-principles calculations, thermodynamics principles, and fuel performance analysis methods, along with our databases.

Advanced Fuel Development

A key technology in the fabrication of nitride fuels for minor actinide (MA) transmutation is the external gelation technique, which enables the preparation of MA nitride particles from MA solutions without powder processes. As a proof-of-concept, we assembled an external gelation system in Research Building No. 4 to prepare gel particles using rare-earth elements as surrogates. The feed solution utilized in this method comprised nitrate, a nanocarbon dispersion, and polyvinyl alcohol. This solution was dropped through a vibrating fine nozzle into an ammonia water bath, where gel particles form. By modulating the feed composition, viscosity, dispenser pressure, and nozzle frequency, we successfully obtained spherical dysprosium (Dy) particles with small diameters (Fig. 1). Following the synthesis of nitride particles through calcination and carbothermic nitridation, we plan to conduct fabrication tests on high-performance heterogeneous fuel pellets with DyN particles dispersed in a titanium nitride matrix.

Additionally, to prepare for the irradiation tests of nitride fuel in the experimental reactor JOYO, we have begun analyzing fuel behavior using the code FEMAXI, which has been improved for nitride fuel analysis.

FP Behavior

Understanding the distribution and water solubility of radioactive cesium (Cs), a major radiation sources within TEPCO's Fukushima Daiichi Nuclear Power Station (1F), is crucial for reasonable safety assessments of the fuel debris retrieval and decommissioning process. To improve the FP chemistry database ECUME, we investigated the Cs chemistry within the reactor, which influences Cs transport during SAs.

Internal investigations of 1F revealed unexpectedly high dose rates in the shield plug above the primary

containment vessel, indicating some trapping of Cs in the concrete of the shield plugs. To probe this, reaction tests of Cs aerosol with concrete at 200°C were performed¹⁾. These tests revealed that Cs-concrete interactions at approximately 200°C led to the formation of water-insoluble Cs-(Al,Fe)-Si-O deposits (Fig. 2), along with water-soluble phases, namely Cs carbonate hydrate and potentially Cs silicate in the absence of Al and Fe. Our findings indicated that Cs may be trapped in the concrete through chemical reactions with CaCO₃, forming Cs₂CO₃ hydrates, and with aluminosilicate and SiO₂, forming Cs-Al-Si-O and Cs-Si-O deposits, respectively. Future improvements to ECUME will incorporate newly obtained data to better estimate Cs trapping in concrete, as well as the Cs distribution in 1F.

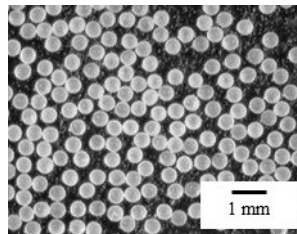


Fig. 1 Dy gel particles prepared using the external gelation technique

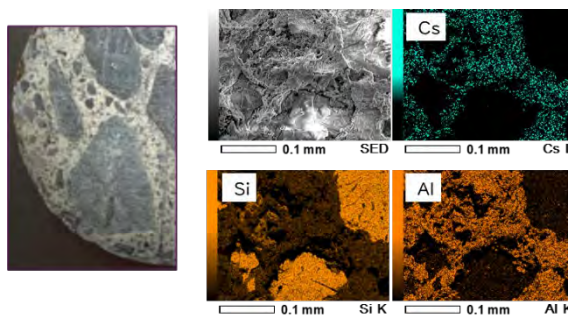


Fig. 2 Appearance of concrete (left) and distribution of Cs, Si, and Al in the concrete aggregate reacted with Cs aerosol at 200°C (right)

Reference

- 1) V. N. Luu, K. Nakajima, *Mech. Eng. J.* 11(2), 23-00446 (2024).



Contact (Group Leader):

MIWA Shuhei

miwa.shuhei@jaea.go.jp

Research Group for Nuclear Fuel Cycle Science

Partitioning and transmutation have been proposed for managing high-level radioactive waste (HLW) generated by reprocessing spent nuclear fuel via hydrometallurgical methods. Notably, HLW comprises numerous elements with varying radiotoxicities and chemical properties, making it reasonable to separate these elements into groups for better management.

To this end, our research group has proposed a novel hydrometallurgical process called Solvent Extraction from Liquid waste using Extractants of CHON-type for Transmutation (SELECT) to recycle nuclear materials and separate actinides. A conceptual flow diagram of SELECT is presented in Fig. 1. The process comprises the following four steps: (i) recovery of U and Pu from the dissolution solution of spent nuclear fuel using monoamides, (ii) recovery of minor actinides (MAs; Am and Cm), and rare earths (REs) from HLW using diglycolamide, (iii) separation of MAs from REs using nitrilotriacetamide, and (iv) separation of Am and Cm using alkyl diamine. The extractants utilized in this process consist of carbon, hydrogen, oxygen, and nitrogen, which can be decomposed into gases by incineration, thereby contributing toward reducing the volume of secondary solid waste.

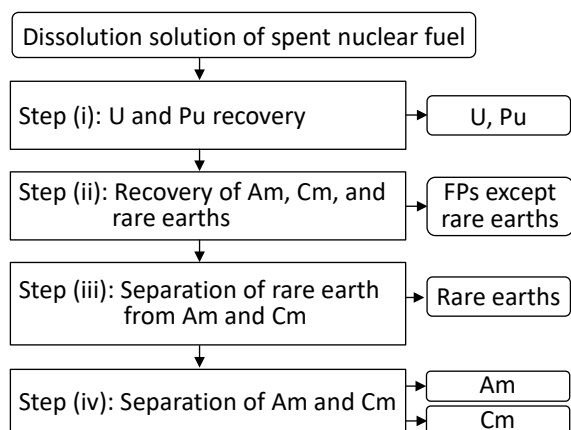


Fig. 1 A conceptual flow diagram of SELECT

A Demonstration Test to Separate MA from HLW in a Hot Cell

Throughout the development of the SELECT process, abundant fundamental data have been collected through experiments conducted using radioactive isotopes and HLW. These data demonstrate that the abovementioned extractants are promising candidates and support the practicality of SELECT. Although a continuous counter-current experiment for step (iii) was

previously conducted with HLW using nitorilotriacetoamide (HONTA), the cumulative duration was limited to 20 h. Hence, a demonstration test was performed for a cumulative duration of 40 h to further evaluate the practicality of HONTA (Fig. 2).

For this test, HLW stored in a hot cell at the Nuclear Fuel Cycle Safety Engineering Research Facility (NUCEF) was used as the feed after recovering MAs and REs using tetradodecyl diglycolamide as the extractant. HONTA diluted with *n*-dodecane was used as the organic phase. Although part of the organic phase was reused without solvent regeneration, no third phase formation or precipitation was observed throughout the experiment.

HONTA effectively extracted MAs, and the extracted MAs was back-extracted by coming into contact with nitric acid of ca. 1 mol/dm³. REs (Y, La, Nd, and Eu) were less extractable, and the ratios of Y, La, Nd, and Eu distributed to a REs fraction were >99.9%, 99.2%, 61.8%, and 81.4%, respectively. The ratios of Am and Cm distributed to a MAs fraction were 86.8% and 74.7%, respectively, and a substantial amount of MA (0.12 g) was recovered in this fraction¹.

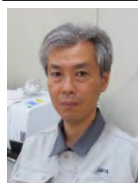
In addition to MAs and REs, HLW contains other valuable metals, including heat-generating elements (Sr and Cs) and noble metals (Ru, Rh, and Pd). Further development of SELECT is underway to enable the separation of these elements.



Fig. 2 Mixer-settler extractors and manipulators used in the demonstration test

Reference

1) Y. Ban, et al., *Solvent Extr. Res. Dev., Jpn.* 31, 1 (2024).



Contact (Group Leader):

BAN Yasutoshi

ban.yasutoshi@jaea.go.jp

Research Group for Environmental Science

Our group investigates the dynamics of radioactive materials in atmospheric, terrestrial, and marine environments to improve the techniques developed for assessing their environmental impacts. In particular, we focus on the development and validation of computer models to predict the dispersion of radioactive materials through the environment. Examples of these models include atmospheric dispersion prediction systems (WSPEEDI-II and WSPEEDI-DB) and an oceanic dispersion prediction system (STEAMER). Furthermore, we conduct field observations to collect environmental samples, particularly from terrestrial and marine environments. These samples are then analyzed using advanced techniques to elucidate the dynamics of radioactive materials and validate our computer models.

Predicting the Discharge of Radioactive Materials from Fukushima River Basins Considering Human Activities

Following the Fukushima Daiichi Nuclear Power Station (1F) accident, ^{137}Cs has accumulated in the seabed sediments of surrounding coastal regions. In particular, ^{137}Cs discharge from rivers to oceans is anticipated to influence the long-term migration of ^{137}Cs in seabed sediments. In a previous study, we implemented a distributed radiocesium prediction model on the Abukuma River basin to predict future ^{137}Cs discharge from this river basin to oceans, considering the characteristics of terrestrial land use¹⁾. In this study, ^{137}Cs discharge from several river basins along the coast of the Fukushima Prefecture to oceans was predicted for the next 30 years, considering human activities²⁾.

The distributed radiocesium prediction model adopted in this study was refined from the previous model to account for sedimentation at dams and erosion and sedimentation in floodplains. The model integrated a hydrological model, sediment transport model, and radiocesium transport model. Four land use categories were established: croplands, forest areas, urban lands, and paddy fields. We also evaluated the impacts of decontamination efforts and the resumption of agriculture on ^{137}Cs discharge. The calculation domain extended within 70 km of 1F, and predictions were made for a 30-year period from January 2011 to December 2040.

Figure 1 illustrates a time series of the accumulated ^{137}Cs amount discharged into rivers from different land use areas in the coastal region of the

Fukushima Prefecture. The results suggest that in the 2.5 years following the 1F accident, runoff from forested areas and urban lands was considerable, following which forest runoff became dominant. Human activities, particularly in croplands and paddy fields, were also predicted to mitigate ^{137}Cs discharge into rivers and oceans. Furthermore, an analysis of the effect of the ^{137}Cs amount discharged from rivers on the ^{137}Cs amount collected in seabed sediments revealed that the ^{137}Cs amount discharged from rivers was 11%–36% of the ^{137}Cs amount accumulated in the early stages of the 1F accident. This underscores the importance of accurately determining the ^{137}Cs discharge from rivers to predict the future migration of ^{137}Cs in seabed sediments around 1F.

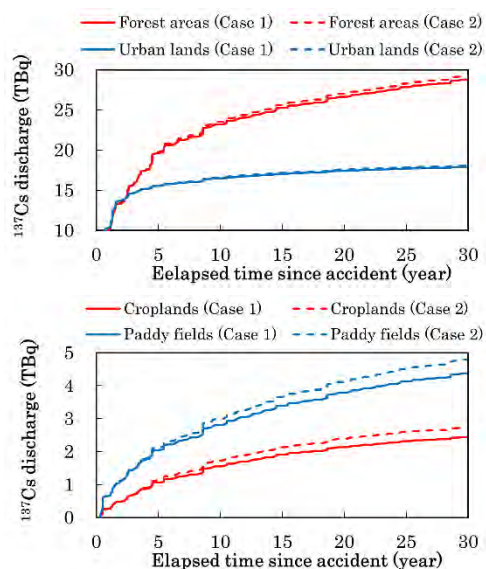


Fig. 1 Time series plots of ^{137}Cs discharged into rivers from the land areas of Fukushima river basins. Cases 1 and 2 display results with and without human activities, respectively.

References

- 1) T. Ikenoue, et al., *Sci. Total Environ.* 876, 162846 (2023), <https://doi.org/10.1016/j.scitotenv.2023.162846>.
- 2) T. Ikenoue, et al., *Water* 15, 2734 (2023), <https://doi.org/10.3390/w15152734>.



Contact (Group Leader):

KAWAMURA Hideyuki

kawamura.hideyuki@jaea.go.jp

Research Group for Radiation Transport Analysis

Computer simulations are essential tools for research and development in nuclear and radiation sciences. The Particle and Heavy Ion Transport code System (PHITS) is a radiation transport simulation code being developed by our group to satisfy the evolving needs of society. We conduct studies on radiological protection and radiation effects. The following description summarizes our progress in FY2023.

Upgrades of the PHITS Code

A new version of PHITS (version 3.34) was developed and released to the public in FY2023. The number of newly registered PHITS users in FY2023 was approximately 1,270, including 530 Japanese users. The followings represent the major upgraded features in the latest version of this code. More detailed information can be found in the PHITS official reference paper¹⁾ and on the homepage²⁾.

Chemical analysis code for PHITS

The PHITS-Chem code³⁾, which enables simulations of the behaviors of radicals generated by water radiolysis, has been incorporated into the PHITS package. This code can estimate the time-dependent yields of radicals that can potentially cause damage to DNA molecules, utilizing the results of the track-structure simulations performed by PHITS.

Extended statistical indicators

The reliability of a Monte Carlo simulation is typically judged by its statistical error, which can be inappropriate when using the variance reduction method. To address this, output functions for extended statistical indicators, such as variance of variance, figure of merit, and probability density function, have been implemented in PHITS. These functions ensure the reliability of PHITS simulation results, particularly for shielding calculations.

RI-production

A method to produce technetium-99m (^{99m}Tc), a radioisotope utilized in medical imaging, by irradiating Mo samples with proton beams in cyclotrons has been proposed to address the supply concerns of aging reactors. In a previous study⁴⁾, we proposed a new method to determine the cross-sections of all Tc isotopes produced by proton-induced reactions on Mo isotopes using data measured with natural Mo. Using this method, the impurity of Tc isotopes other than ^{99m}Tc was reliably

estimated. This implies that our method will help determine appropriate Mo isotopic compositions to obtain ^{99m}Tc products with low impurity levels that meet medical use requirements⁴⁾.

Radiological Research (Mesh Phantom)

Polygon mesh-type phantoms of Japanese reference female (JPF) and male (JPM) were developed for use in dosimetry to reflect individual characteristics, such as posture and body size. Figure 1 illustrates the detailed eye model incorporated into the JPF and JPM. Notably, these phantoms realistically reproduce the eye structure (lens, cornea, aqueous humor, and vitreous), which could not be modeled in previous phantoms. In particular, the sensitive region of the lens is defined to calculate exposure doses based on the latest ICRP (International Commission on Radiological Protection) dosimetry method. These newly developed JPF and JPM are anticipated to contribute to the realization of more accurate dose control for the lenses of both patients and practitioners in medical radiation treatment, which requires careful consideration of posture and body size.

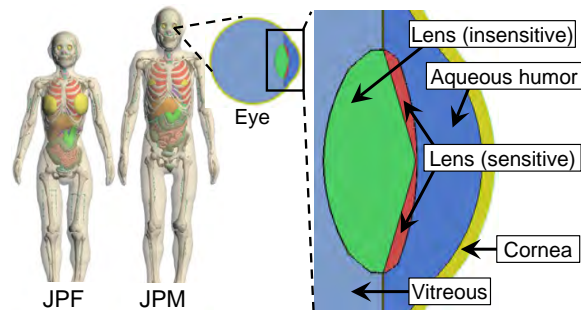


Fig. 1 Cross sectional view of the detailed eye model in the JPF and JPM

References

- 1) T. Sato, et al., *J. Nucl. Sci. Technol.* 61, 127 (2024).
- 2) <https://phits.jaea.go.jp/index.html>.
- 3) Y. Matsuya, et al., *Phys. Med. Biol.* 69, 035005 (2024).
- 4) S. Hashimoto, et al., *J. Phys. Soc. Jpn.* 92, 124202 (2023).



Contact (Group Leader):
TSUDA Shuichi
tsuda.shuichi@jaea.go.jp

Research Group for Nuclear Chemistry

Elucidating the chemical reactions and states of radionuclides in solutions is crucial for addressing various challenges in the nuclear field, particularly in the back-end processes for the safe treatment and disposal of nuclear waste. Our objective is to elucidate the complex reactions of nuclear materials and radiation to predict the behaviors of radionuclides in solutions and the environment. This year, we examined the dissolution and deposition of uranium under redox conditions, where the valence of uranium changes.

Oxidative Dissolution of UO_2 , Dependence on Temperature

The direct disposal of spent nuclear fuel in deep underground repositories is a potential alternative to vitrified radioactive waste. In case of spent-fuel canister failure, potential contact between the fuel and groundwater is anticipated. Under such conditions, water radiolysis generates oxidants. These oxidants, primarily H_2O_2 , induce the dissolution of the UO_2 matrix of spent fuel. Temperature is an important factor in chemical reaction modeling; however, its effect on oxidative dissolution remains unknown. Therefore, we investigated the temperature dependence of H_2O_2 -induced oxidative dissolution of UO_2 . Our experimental results revealed that higher temperatures accelerated surface oxidation; however, the dissolution of oxidized U was limited by its solubility. When dissolution was facilitated by high concentrations of carbonate ions, which form soluble complexes with uranyl ions, high temperatures accelerated U dissolution. However, under low carbonate concentrations and high temperatures, a substantial amount of H_2O_2 decomposed catalytically without U oxidation. Figure 1 illustrates the reaction mechanism at elevated temperatures proposed based on our results.¹⁾ These findings serve as a basis for developing a spent-fuel dissolution model incorporating the temperature dependence.

Uranium Hydroxide/Oxide Deposition Following Uranyl Reduction

Understanding U deposition in the environment is essential for evaluating the safety of the geological disposal of high-level radioactive waste. However, the precise mechanism underlying deposit formation remains unclear. We investigated the chemical reactions within deposits following the

reduction of uranyl ions (U(VI)O_2^{2+}) using electrochemical quartz crystal microbalance, impedance spectra, and X-ray absorption fine-structure measurements²⁾. Based on these results, we proposed the following deposition mechanism (Fig. 2). (i) U(VI) is reduced to U(V) under reducing conditions, and U(IV) is formed by the disproportionation of U(V) . (ii) U(IV) forms U(IV) hydroxide deposits, which catalyze the reduction of U(V) . (iii) Finally, the hydroxide deposits transform into U(IV) oxides, which generally exhibit greater electrical resistance than hydroxides. This is the first report elucidating the deposition mechanism following U reduction.

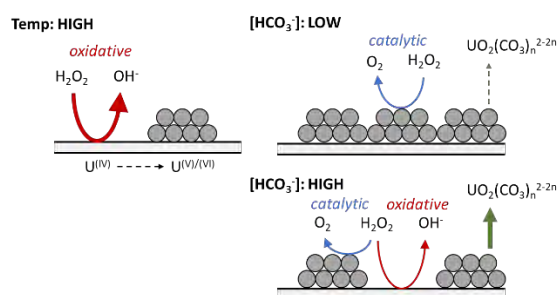


Fig. 1 Proposed model of H_2O_2 -induced UO_2 dissolution at elevated temperatures

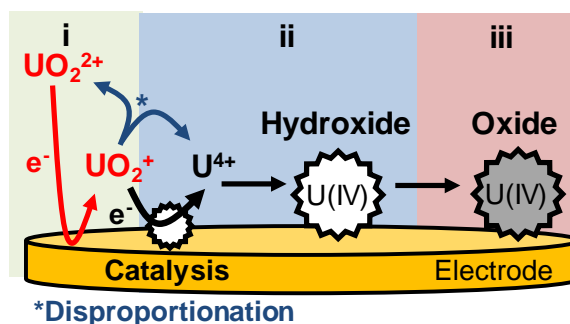


Fig. 2 Proposed mechanism of U electro-deposition

References

- 1) J. McGrady, et al., *RSC Adv.* 13, 28021 (2023).
- 2) K. Ouchi, et al., *RSC Adv.* 13, 16321 (2023).



Contact (Group Leader):

KITATSUJI Yoshihiro

kitatsuji.yoshihiro@jaea.go.jp

Publication list

Nuclear Science and Reactor Engineering Division

Nuclear Data Center

Papers

- 1) Nuclear many-body effects on particle emission following muon capture on Si-28 and Ca-40, F. Minato, T. Naito & O. Iwamoto, *Phys. Rev. C* 107(5), 054314 (2023).
- 2) Measurements of capture cross-section of Nb-93 by activation method and half-life of Nb-94 by mass analysis, S. Nakamura, Y. Shibahara, S. Endo & A. Kimura, *J. Nucl. Sci. Technol.* 60(11), 1361 (2023).
- 3) Deuteron and alpha sub-libraries of JENDL-5, S. Nakayama, O. Iwamoto & J.-C. Sublet, *EPJ Web of Conf.* 284, 14011 (2023).
- 4) General-purpose nuclear data library JENDL-5 and to the next, O. Iwamoto, N. Iwamoto, S. Kunieda, F. Minato, S. Nakayama, A. Kimura, S. Nakamura, S. Endo, Y. Nagaya, K. Tada, C. Konno, N. Matsuda, K. Yokoyama, H. Taninaka, A. Oizumi & S. Okita, *EPJ Web of Conf.* 284, 14001 (2023).
- 5) Neutron filtering system for neutron capture cross section measurement at the ANNRI beamline of MLF/J-PARC, G. Rovira, A. Kimura, S. Nakamura, S. Endo, O. Iwamoto, N. Iwamoto, T. Katabuchi, Y. Kodama, H. Nakano, J.-i. Hori, Y. Shibahara & K. Terada, *EPJ Web of Conf.* 284, 06007 (2023).
- 6) Present status of an R-matrix analysis code AMUR for cross-section evaluation in resolved resonance region, S. Kunieda, *EPJ Web of Conf.* 284, 03014 (2023).
- 7) Simulated performance evaluation of d-Be compact fast neutron source, S. Nakayama, *J. Nucl. Sci. Technol.* 60(12), 1447 (2023).
- 8) Measurements of the neutron total and capture cross sections and derivation of the resonance parameters of Ta-181, S. Endo, A. Kimura, S. Nakamura, O. Iwamoto, N. Iwamoto, G. Rovira, Y. Toh, M. Segawa & M. Maeda, *Nucl. Sci. Eng.* 198(4), 786 (2024).
- 9) Am-241 neutron capture cross section measurement using the NaI(Tl) spectrometer of the ANNRI beamline of J-PARC, G. Rovira, A. Kimura, S. Nakamura, S. Endo, O. Iwamoto, N. Iwamoto, T. Katabuchi, Y. Kodama, H. Nakano & Y. Sato, *J. Nucl. Sci. Technol.* 61(4), 459 (2024).
- 10) Measurements of neutron total and capture cross sections of La-139 and evaluation of resonance parameters, S. Endo, S. Kawamura, T. Okudaira, H. Yoshikawa, G. Rovira, A. Kimura, S. Nakamura, O. Iwamoto & N. Iwamoto, *Eur. Phys. J. A* 59, 288 (2023).
- 11) JENDL-5 benchmarking for fission reactor applications, K. Tada, Y. Nagaya, H. Taninaka, K. Yokoyama, S. Okita, A. Oizumi, M. Fukushima & S. Nakayama, *J. Nucl. Sci. Technol.* 61(1), 2 (2024).
- 12) Development of correction method for sample density effect on PGA, M. Maeda, M. Segawa, Y. Toh, S. Endo, S. Nakamura & A. Kimura, *J. Radioanal. Nucl. Chem.* 332(8), 2995 (2023).
- 13) Simultaneous evaluation of uranium and plutonium fast neutron fission cross sections up to 200 MeV for JENDL-5 and its updates, N. Otuka & O. Iwamoto, *EPJ Web of Conf.* 284, 08011 (2023).
- 14) Neutron capture cross section measurement and resonance analysis of Pd-107 using ANNRI at MLF/J-PARC, H. Nakano, T. Katabuchi, K. Terada, A. Kimura, S. Nakamura, S. Endo, G. Rovira & Y. Kodama, *EPJ Web of Conf.* 284, 01032 (2023).
- 15) Measurement of the $^{235}\text{U}(n,f)$ cross section relative to the $^{10}\text{B}(n,\alpha)$ reaction with Micromegas detectors at the CERN n_TOF facility: first results, V. Michalopoulou, et al. (The n_TOF Collaboration (H. Harada & A. Kimura)), *EPJ Web of Conf.* 284, 01030 (2023).
- 16) Measurements of the neutron capture cross section of Am-243 with the ANNRI beamline, MLF/J-PARC, Y. Kodama, T. Katabuchi, G. Rovira, A. Kimura, S. Nakamura, S. Endo, H. Nakano, Y. Sato, J.-i. Hori, Y. Shibahara & K. Terada, *EPJ Web of Conf.* 284, 01024 (2023).
- 17) Neutron production in the interaction of 200-MeV deuterons with Li, Be, C, Al, Cu, Nb, In, Ta, and Au, Y. Watanabe, H. Sadamatsu, S. Araki, K. Nakano, S. Kawase, T. Kin, Y. Iwamoto, D. Satoh, M. Hagiwara, H. Yashima, T. Shima & S. Nakayama, *EPJ Web of Conf.* 284, 01041 (2023).
- 18) Evaluation of the production amount of Ac-225 and its uncertainty through the $^{226}\text{Ra}(n,2n)$ reaction in the experimental fast reactor Joyo, Y. Sasaki, A. Sano, S. Sasaki, N. Iwamoto, K. Ouchi,

- Y. Kitatsuji, N. Takaki & S. Maeda, *J. Nucl. Sci. Technol.* 61(4), 509 (2024).
- 19) Status of the Ra-226 nuclear data library and its impact on the production amount of Ac-225 via the ^{226}Ra (n,2n) reaction, Y. Sasaki, N. Iwamoto, N. Takaki & S. Maeda, *J. Nucl. Sci. Technol.* 61(2), 251 (2024).
- 20) Measurement of the neutron capture cross section of ^{185}Re in the keV energy region, T. Katabuchi, Y. Sato, K. Takebe, M. Igashira, S. Umezawa, R. Fujioka, T. Saito & N. Iwamoto, *J. Nucl. Sci. Technol.* 61(2), 224 (2024).
- 21) FENDL: A library for fusion research and applications, G. Schnabel, D.L. Aldama, T. Bohm, U. Fischer, S. Kunieda, A. Trkov, C. Konno, R. Capote, A.J. Koning, S. Breidokaite, T. Eade, M. Fabbri, D. Flammini, L. Isolan, I. Kodeli, M. Košťál, S. Kwon, D. Laghi, D. Leichtle, S. Nakayama, M. Ohta, L.W. Packer, Y. Qiu, S. Sato, M. Sawan, M. Schulc, G. Stankunas, M. Sumini, A. Valentine, R. Villari & A. Žohar, *Nucl. Data Sheets* 193, 1 (2024).
- 22) PR8-3 Neutron capture cross-section measurements with TC-Pn in KUR for some nuclides targeted for decommissioning, S. Nakamura, S. Endo, A. Kimura & Y. Shibahara, *KURNS PROGRESS REPORT 2022*, 73 (2023).
- 23) Application for the epithermal polarized neutron beam at ANNRI in J-PARC, S. Endo & T. Okudaira, *波紋 Hamon* 33(2), 68 (2023) (*in Japanese*).

JAEA Reports

- 1) Neutron capture cross section measurement of ^{129}I and ^{127}I using ANNRI at MLF/J-PARC, G. Rovira, A. Kimura, S. Nakamura, S. Endo, O. Iwamoto, N. Iwamoto, Y. Toh, M. Segawa, M. Maeda & T. Katabuchi, *JAEA-Conf 2023-001*, 74 (2024).
- 2) Extension of R-matrix code AMUR toward analysis on actinide nuclei - a feasibility study on U-233 -, S. Kunieda, *JAEA-Conf 2023-001*, 138 (2024).

Research Group for Nuclear Sensing

Papers

- 1) Development of an integrated non-destructive analysis system, Active-N, H. Tsuchiya, Y. Toh, A. Ohzu, K. Furutaka, F. Kitatani, M. Maeda & M. Komeda, *J. Nucl. Sci. Technol.* 60(11), 1301 (2023).
- 2) Development of correction method for sample density effect on PGA, M. Maeda, M. Segawa, Y. Toh, S. Endo, S. Nakamura & A. Kimura, *J. Radioanal. Nucl. Chem.* 332, 2995 (2023).
- 3) Development of a DDA+PGA-combined non-destructive active interrogation system in "Active-N", K. Furutaka, A. Ohzu & Y. Toh, *Nucl. Eng. Technol.* 55(11), 4002 (2023).
- 4) Measurements of the neutron total and capture cross sections and derivation of the resonance parameters of Ta-181, S. Endo, A. Kimura, S. Nakamura, O. Iwamoto, N. Iwamoto, G. Rovira, Y. Toh, M. Segawa & M. Maeda, *Nucl. Sci. Eng.* 198(4), 786 (2024).
- 5) Termination of downward-oriented gamma-ray glow by normal-polarity in-cloud discharge activity, Y. Wada, T. Wu, D. Wang, T. Enoto, K. Nakazawa, T. Morimoto, Y. Nakamura, T. Shinoda & H. Tsuchiya, *J. of Geophys. Res.: Atmospheres* 128(15), e2023JD038606_1 - e2023JD038606_9 (2023).
- 6) Citizen science observation of a gamma-ray glow associated with the initiation of a lightning flash, M. Tsurumi, T. Enoto, Y. Ikkatai, T. Wu, D. Wang, T. Shinoda, K. Nakazawa, N. Tsuji, G. S. Diniz, J. Kataoka, N. Koshikawa, R. Iwashita, M. Kamogawa, T. Takagaki, S. Miyake, D. Tomioka, T. Morimoto, Y. Nakamura & H. Tsuchiya, *Geophys. Res. Lett.* 50(13), e2023GL103612_1 - e2023GL103612_9 (2023).
- 7) Negative excursion of surface electric fields during gamma-ray glows in winter thunderstorms, Y. Wada, M. Kamogawa, M. Kubo, T. Enoto, S. Hayashi, T. Sawano, D. Yonetoku & H. Tsuchiya, *J. of Geophys. Res.: Atmospheres* 128(21), e2023JD039354_1 - e2023JD039354_20 (2023).
- 8) Observation of gamma rays up to 320 TeV from the middle-aged TeV pulsar wind nebula HESS J1849-000, M. Amenomori, (H. Tsuchiya) et. al., *Astrophys. J.* 954(200), 200_1 - 200_7 (2023).
- 9) CO8-1 Demonstration experiment of detecting the HEU sample using a low-cost inspection

system, M. Komeda, K. Tanabe, Y. Toh, Y. Kitamura & T. Misawa, *KURNS PROGRESS*

REPORT 2022, 222 (2023).

Patents

- 1) M. Komeda & Y. Toh, "Nuclear substance detection device, nuclear substance detection method, and sample analysis method", Japanese Patent 7281816 (2023.05.18)
- 2) M. Maeda, Y. Toh & M. Komeda, "Material detection device", Japanese Patent 7287736 (2023.05.29)

Research Group for Reactor Physics and Thermal-Hydraulics Technology

Papers

- 1) JENDL-5 benchmarking for fission reactor applications, K. Tada, Y. Nagaya, H. Taninaka, K. Yokoyama, S. Okita, A. Oizumi, M. Fukushima & S. Nakayama, *J. Nucl. Sci. Technol.* 61(1), 2 (2024).
- 2) Convergence behavior of statistical uncertainty in probability table for cross section in unresolved resonance region, K. Tada & T. Endo, *J. Nucl. Sci. Technol.* 60(11), 1397 (2023).
- 3) Statistical uncertainty quantification of probability tables for unresolved resonance cross sections, K. Tada & T. Endo, *EPJ Web of Conf.* 284, 14013 (2023).
- 4) Analyses of JAEA/FNS iron in-situ experiment with latest nuclear data libraries, C. Konno & S. Kwon, *EPJ Web of Conf.* 284, 15010 (2023).
- 5) Development of a numerical simulation method for air cooling of fuel debris by JUPITER, S. Yamashita, S. Uesawa, A. Ono & H. Yoshida, *Mech. Eng. J.* 10(4), 22-00485 (2023).
- 6) Atomization mechanisms of a wall-impinging jet in a shallow pool, N. Horiguchi, H. Yoshida, A. Kaneko & Y. Abe, *Phys. Fluids* 35, 073309 (2023).
- 7) Measurement of the water-vapor void fraction in a 4 × 4 unheated rod bundle, T. Nagatake & H. Yoshida, *J. Nucl. Sci. Technol.* 60(11), 1417 (2023).
- 8) New JENDL-4.0/HE neutron and proton ACE files, C. Konno, *J. Nucl. Sci. Technol.* 61(1), 121 (2024).
- 9) Neutron importance estimation via new recursive Monte Carlo method for deep penetration neutron transport, D. Tuya & Y. Nagaya, *J. Nucl. Sci. Eng.* 198(5), 1021 (2023).
- 10) Benchmark simulation code for the thermal-hydraulics design tool of the accelerator-driven system: validation and benchmark simulation of flow behavior around the beam window, S. Yamashita, N. Kondo, T. Sugawara, H. Monji & H. Yoshida, *J. Nucl. Sci. Technol.* 61(6), 740 (2024).
- 11) Estimation of continuous distribution of iterated fission probability using an artificial neural network with Monte Carlo-based training data, D. Tuya & Y. Nagaya, *J. Nucl. Eng.* 4(4), 691 (2023).
- 12) Development of nuclear data processing code FRENDY version 2, K. Tada, A. Yamamoto, S. Kunieda, C. Konno, R. Kondo & T. Endo, *J. Nucl. Sci. Technol.* 61(6), 830 (2024).
- 13) Generation and verification of ORIGEN and ORIGEN-S activation cross-section libraries of JENDL-5 and JENDL/AD-2017, C. Konno, M. Kochiyama & H. Hayashi, *Mech. Eng. J.* 11(2), 23-00386 (2024).
- 14) Impact of nuclear data revised from JENDL-4.0 to JENDL-5 on PWR spent fuel nuclide composition, T. Watanabe, K. Tada, T. Endo & A. Yamamoto, *J. Nucl. Sci. Technol.* 60(11), 1386 (2023).
- 15) General-purpose nuclear data library JENDL-5 and to the next, O. Iwamoto, N. Iwamoto, S. Kunieda, F. Minato, S. Nakayama, A. Kimura, S. Nakamura, S. Endo, Y. Nagaya, K. Tada, C. Konno, N. Matsuda, K. Yokoyama, H. Taninaka, A. Oizumi & S. Okita, *EPJ Web of Conf.* 284, 14001 (2023).
- 16) FENDL: A library for fusion research and applications, G. Schnabel, D.L. Aldama, T. Bohm, U. Fischer, S. Kunieda, A. Trkov, C. Konno, R. Capote, A.J. Koning, S. Breidokaite, T. Eade, M. Fabbri, D. Flammini, L. Isolani, I. Kodeli, M. Košťál, S. Kwon, D. Laghi, D. Leichtle, S. Nakayama, M. Ohta, L.W. Packer, Y. Qiu, S. Sato, M. Sawan, M. Schulc, G. Stankunas, M. Sumini, A. Valentine, R. Villari & A. Žohar, *Nucl. Data Sheets* 193, 1 (2024).
- 17) Whole core analysis of BEAVRS benchmark for hot zero power condition using MVP3 with JENDL-5, M. Suzuki & Y. Nagaya, *J. Nucl. Sci. Technol.* 61(2), 177 (2024).
- 18) Breakup of single droplet induced by high Weber number flow behind shock wave, M. Asahara, K. Iwasaki, T. Kamiya, K. Mizuno, K. Iwasaki & T. Miyasaka, *Japanese J. Multiphase Flow* 38(2), 175 (2024).

- 19) Initial verification and validation of a new CASMO5 JENDL-5 nuclear data library for typical LWR applications, T. Watanabe, K. Suyama, K. Tada, R. M. Ferrer, J. Hykes & C. A. Wemple, *Nucl. Sci. Eng.* 198(11), 2230 <https://doi.org/10.1080/00295639.2023.2295075> (2024).
- 20) ORIGEN and ORIGEN-S libraries produced from JENDL-5, C. Konno, M. Kochiyama & H. Hayashi, *Proc. 30th International Conference on Nuclear Engineering (ICONE30)* (2023).
- 21) Approximate estimation of iterated fission probability by deep neural network, D. Tuya & Y. Nagaya, *Proc. 30th International Conference on Nuclear Engineering (ICONE30)* (2023).
- 22) Development of numerical simulation method of natural convection around heated porous medium by using JUPITER, S. Uesawa, S. Yamashita, M. Shibata & H. Yoshida, *Proc. 30th International Conference on Nuclear Engineering (ICONE30)* (2023).
- 23) Experiment and numerical simulation of pulsation flow in single channel for Li-7 enrichment technology development by MCCCE method, H. Horiguchi, H. Yoshida, Y. Kitatsuji, M. Hasegawa & T. Kishimoto, *Proc. 30th International Conference on Nuclear Engineering (ICONE30)* (2023).
- 24) A Functional expansion tally method with numerical basis sets generated by singular value decomposition for one-dimensional Monte Carlo calculations, R. Kondo & Y. Nagaya, *Proc. International Conference on Mathematics and Computational Methods Applied to Nuclear Science and Engineering (M&C 2023)* (2023).
- 25) Measurement of void fraction distribution at high pressure in 4×4 simulated fuel bundle for validation of thermal-hydraulics simulation codes, T. Nagatake, M. Shibata, S. Uesawa, A. Ono & H. Yoshida, *第27回動力・エネルギー技術シンポジウム講演論文集 (The 27th National Symposium on Power and Energy Systems)* (2023) (in Japanese).
- 26) Comparison of neutronic characteristics of BWR burnup fuel between JENDL-4.0 and JENDL-5, T. Watanabe, K. Tada, T. Endo & A. Yamamoto, *Proc. 12th International Conference on Nuclear Criticality Safety (ICNC2023)* (2023).
- 27) Linearization of thermal neutron scattering cross section to optimize the number of energy grid points, K. Tada, *Proc. 12th International Conference on Nuclear Criticality Safety (ICNC2023)* (2023).
- 28) Development of sharp-interface method based on conservation law for liquid-gas two-phase compressible fluid simulations, T. Kamiya & H. Yoshida, *第37回数値流体力学シンポジウム講演論文集 (37th CFD Symposium)* (2023) (in Japanese).
- 29) Development of the ghost fluid method satisfying conservation laws for liquid-gas flow with shock wave, T. Kamiya & H. Yoshida, *衝撃波シンポジウム講演論文集 (Symposium on Shock Waves in Japan)* (2024) (in Japanese).

JAEA Report

- 1) Processing of JENDL-5 photonuclear sublibrary, C. Konno, *JAEA-Conf 2023-001*, 143 (2024).

Patent

- 1) S. Uesawa, "Purification method of gas, and purifier therefor", Japanese Patent 7320708 (2023.07.27)

Research Group for Nuclear Transmutation System

Papers

- 1) Nuclide production cross sections in proton-induced reactions on Bi at GeV energies, H. Iwamoto, K. Nakano, S.-i. Meigo, H. Takeshita & F. Maekawa, *EPJ Web of Conf.* 284, 01033 (2023).
- 2) Neutron-production double-differential cross sections of ^{nat}Pb and ^{209}Bi in proton-induced reactions near 100 MeV, H. Iwamoto, S. Meigo, D. Satoh, Y. Iwamoto, Y. Ishi, T. Uesugi, H. Yashima, K. Nishio, K. Sugihara, Y. Çelik & A. Stankovskiy, *Nuclear Instruments and Methods in Physics Research B*, 544, 165107_1-165107_15 (2023).
- 3) TRU oxide sample reactivity worths measured in the FCA-IX assemblies with systematically changed neutron energy spectra, M. Fukushima, S. Okajima & T. Mukaiyama, *J. Nucl. Sci. Technol.* 61(4), 478-497 (2023).

- 4) Direct disposal concepts of spent mixed oxide fuel from light water reactors based on heat transfer calculations, T. Abe & K. Nishihara, *J. Nucl. Sci. Technol.* 61(8), 1048-1060 (2024).
- 5) Impact of uncertainty reduction on lead-bismuth coolant in accelerator-driven system using sample reactivity experiments, R. Katano, A. Oizumi, M. Fukushima, C. H. Pyeon, A. Yamamoto & T. Endo, *Nuclear Science and Engineering*, 198(6), 1215-1234 (2023).
- 6) Development of numerical analysis method of oxide layers growth and dissolution rates at wall of lead-bismuth eutectic channel, N. Kondo, K. Nishihara & H. Yoshida, *Proc. 20th International Topical Meeting on Nuclear Reactor Thermal Hydraulics (NURETH-20)* 3522-3534 (2023).
- 7) Impact of using JENDL-5 on neutronics analysis of transmutation systems, T. Sugawara & S. Kunieda, *Proc. International Conference on Mathematics and Computational Methods Applied to Nuclear Science and Engineering (M&C 2023) (Internet)*. (2023)
- 8) Misuse scenario analysis of accelerator-driven system and the effects of dual C/S and design information verification, A. Oizumi & H. Sagara, *第44回日本核物質管理学会年次大会会議論文集(インターネット)* (2023) (*in Japanese*).
- 9) Void reactivity in lead and bismuth sample reactivity experiments at Kyoto University Critical Assembly, C. H. Pyeon, R. Katano, A. Oizumi & M. Fukushima, *Nuclear Science and Engineering*, 197(11), 2902-2919 (2023).

JAEA Reports

- 1) Neutron flux estimation and neutronics characteristics calculation in post-JMTR conceptual study, A. Oizumi & H. Akie, *JAEA-Technology* 2023-017(2023) (*in Japanese*).
- 2) Measurement of 100 MeV-range nuclear reaction data using the fixed-field alternating gradient accelerator at Kyoto University, H. Iwamoto, *JAEA-Conf* 2023-001, 40-45 (2023)

Fuels and Materials Engineering Division

Research Group for Corrosion Resistant Materials

Papers

- 1) Synergistic effect of aluminum lactate and sodium molybdate on freshwater corrosion of carbon steel under irradiation, K. Otani, C. Kato & T. Igarashi, *Corrosion*, 79(11), 1277 (2023).
- 2) Effects of the low-oxygen gas-phase radiolysis on the corrosive environment in the liquid phase, K. Hata, A. Kimura, M. Taguchi, T. Sato, C. Kato & Y. Watanabe, *Zairyo-to-Kankyo*, 72(4), 126 (2023) (*in Japanese*).

JAEA Report

- 1) Development of an electrochemical measurement method for carbon steels in radiation source dissolved solution and a corroded specimen analysis method using an imaging plate, N. Yamashita, T. Aoyama, C. Kato, N. Sano & S. Tagami, *JAEA-Technology*, 2023-028 (2023) (*in Japanese*).

Research Group for Radiation Materials Engineering

Papers

- 1) Alloy design and characterization of a recrystallized FeCrAl-ODS cladding for accident-tolerant BWR fuels: an overview of research activity in Japan, S. Ukai, K. Sakamoto, S. Ohtsuka, S. Yamashita & A. Kimura, *J. Nucl. Mater.* 583, 154508 (2023).
- 2) Time-lapse observation of crevice corrosion in grade 2205 duplex stainless steel, S. Aoki & D.L.

- Engelberg, *Materials* 16(15), 5300 (2023).
- 3) Ion tracks and nanohillocks created in natural zirconia irradiated with swift heavy ions, N. Ishikawa, S. Fukuda, T. Nakajima, H. Ogawa, Y. Fujimura & T. Taguchi, *Materials* 17(3), 547 (2024).
 - 4) Intrinsic factors responsible for brittle versus ductile nature of refractory high-entropy alloys, T. Tsuru, S. Han, S. Matsuura, Z. Chen, K. Kishida, I. Lobzenko, S. I. Rao, C. Woodward, E. P. George & H. Inui, *Nature Commun.* 15, 1706 (2024).
 - 5) First-principles analysis of the effects of oxygen, vacancy and their complex on screw dislocation motion in BCC Nb, T. Tsuru, I. Lobzenko, S. Ogata & W.-Z. Han, *J. Mater. Res. Tech.* 28, 1013–1021 (2024).
 - 6) Implementation of atomic stress calculations with artificial neural-network potentials, I. Lobzenko, T. Tsuru, H. Mori, D. Matsunaka & Y. Shiihara, *Mater. Trans.* 64, 2481–2488 (2023).
 - 7) First-principles atomic level stresses: application to a metallic glass under shear, I. Lobzenko, T. Tsuru, Y. Shiihara & T. Iwashita, *Mater. Res. Expr.* 10, 085201 (2023).
 - 8) Positron annihilation lifetime spectroscopy of FeCr and FeCrAl oxide dispersion strengthened (ODS) alloys, S. Ukai, T. Hirade & N. Okubo, *Materials Characterization* 211, 113813 (2024).
 - 9) Behavior of FeCrAl-ODS cladding tube under loss-of-coolant accident conditions, T. Narukawa, K. Kondo, Y. Fujimura, K. Kakiuchi, Y. Udagawa & Y. Nemoto, *J. Nucl. Mater.* 582, 154467 (2023).
 - 10) Oxidation and embrittlement behavior of FeCrAl-ODS cladding tube under loss-of-coolant accident conditions, T. Narukawa, K. Kondo, Y. Fujimura, K. Kakiuchi, Y. Udagawa & Y. Nemoto, *J. Nucl. Mater.* 587, 154736 (2023).
 - 11) Large-scale atomistic simulations of cleavage in BCC Fe using machine-learning potential, T. Suzudo, K. Ebihara, T. Tsuru & H. Mori, *Zairyo* 73, 129–135 (2024) (*in Japanese*).
 - 12) Emergence of crack tip plasticity in semi-brittle α -Fe, T. Suzudo, K. Ebihara, T. Tsuru & H. Mori, *J. Appl. Phys.* 135, 075102 (2024).
 - 13) Grain boundary plasticity in Mg binary alloys by segregation of p-block element, H Somekawa, T. Tsuru & A. Singh, *Mater. Sci. Eng. A* 893, 146066 (2024).
 - 14) Temperature dependence of deformation and fracture in a beta titanium alloy of Ti-22V-4Al, M. Tanaka, S. Yamasaki, T. Morikawa & T. Tsuru, *Keikinzoku* 73(10), 497–503 (2023) (*in Japanese*).
 - 15) First-principles calculations of hydrogen trapping energy on incoherent interfaces of aluminum alloys, M. Yamaguchi, K. Ebihara, T. Tsuru & M. Itakura, *Mater. Trans.* 64, 2553–2559 (2023).
 - 16) Effects of local bonding between solute atoms and vacancy on formation of nanoclusters in Al-Mg-Si alloys, K. Kurihara, I. Lobzenko, T. Tsuru & A. Serizawa, *Mater. Trans.* 64, 1930–1936 (2023).
 - 17) Oxygen interstitials make metastable β titanium alloys strong and ductile, Y. Chong, R. Cholzadeh, B. Guo, T. Tsuru, G. Zhao, S. Yoshida, M. Mitsuhashi, A. Godfrey & N. Tsuji, *Acta Mater.* 257, 119165 (2023).
 - 18) Dynamic interaction between dislocations and obstacles in bcc iron based on atomic potentials derived using neural networks, H. Mori, T. Tsuru, M. Okumura, D. Matsunaka, Y. Shiihara & M. Itakura, *Phys. Rev. Mater.* 7, 063605 (2023).
 - 19) Existence of hexagonal tabular β -phase in Al-Mg-Si alloys containing noble metal elements, T. Tsuchiya, K. Uttarasak, S. Lee, A. Ahmed, Š. Mikmeková, K. Nishimura, N. Nunomura, K. Shmizu, K. Hirayama, H. Toda, M. Yamaguchi, T. Tsuru, J. Nakamura, S. Ikeno & K. Matsuda, *Mater. Today Commun.* 35, 106198 (2023).
 - 20) Mineral detection of neutrinos and dark matter. A whitepaper, S. Baum, et al. (33rd author: N. Ishikawa), *Physics of the Dark Universe*, 41, 101245 (2023).
 - 21) Influence of defect morphology on absolute J_c value in heavy-ion irradiated REBCO films, T. Sueyoshi, T. Ozaki, S. Semboshi, H. Sakane, T. Nishizaki & N. Ishikawa, *IEEE Trans. Appl. Supercond.* 33, 6600305 (2023).
 - 22) Transition of the $Zr(Cr, Fe)_2$ intermetallic phase up to the eutectic temperature, A. Mohamad, Y. Nemoto, K. Furumoto, Y. Okada & D. Sato, *Proc. 28th International QUENCH Workshop, 5-7 December 2023, Karlsruhe Institute of Technology* (2023).

Research Group for High Temperature Science on Fuel Materials

Papers

- 1) Microstructural evolution of intermetallic phase precipitates in Cr-coated zirconium alloy

- cladding in high-temperature steam oxidation up to 1400°C, A. Mohamad, Y. Nemoto, K. Furumoto, Y. Okada & D. Sato, *Corrosion Science* 224, 111540 (2023).
- 2) Surface analyses of CsOH chemisorbed on concrete and aggregate at around 200°C, V. N. Luu & K. Nakajima, *Proc. ICONE30*, 1940 (2023).
 - 3) Characterization of Cs deposits formed by the interaction of simulated fission product CsOH in the gas phase and concrete at 200°C, V. N. Luu & K. Nakajima, *Mech. Eng. J.* 11(2), 23-00446 (2024).
 - 4) Effect of molybdenum release on UO₂/MOX fuel oxidation under severe light water reactor accident conditions, J. Z. Liu, S. Miwa, H. Karasawa & M. Osaka, *Nucl. Mater. Energy* 37, 101532 (2023).
 - 5) Cohesive/adhesive strengths of CsOH-chemisorbed SS304 surfaces, N. Li, Y. Sun, K. Nakajima & K. Kurosaki, *J. Nucl. Sci. Technol.* 61 (3), 343-353 (2024).
 - 6) Uranium hydroxide/oxide deposits on uranyl reduction, K. Ouchi, D. Matsumura, T. Tsuji, T. Kobayashi, H. Otake & Y. Kitatsuji, *RSC Adv.* 13(24), 16321 (2023).
 - 7) Axial variations of oxide layer growth and hydrogen uptake of BWR fuel claddings under steam starvation conditions, K. Sakamoto, M. Adachi, K. Tokushima, M. Aomi, H. Shibata, Y. Nagae & M. Kurata, *Zirconium in the Nuclear Industry; 20th International Symposium (ASTM STP 1645)*, 411-432 (2023).
 - 8) Alteration of fuel debris simulants by *Bacillus subtilis*, J. Liu, Y. Dotsuta, T. Kitagaki, N. Aoyagi, H. Mei, M. Takano & N. Kozai, *J. Nucl. Sci. Technol.* 60 (8), 1002-1012 (2023).
 - 9) Local structure analysis of DyN-ZrN solid solutions, Y. Yoneda, T. Tsuji, D. Matsumura, Y. Okamoto, S. Takaki & M. Takano, *Physica B; Condensed Matter*, 663, p.414960_1 - 414960_9 (2023).
 - 10) Chemical species of cesium and iodine in condensed vaporized microparticles formed by melting nuclear fuel components with concrete materials, T. Onuki, J. Ye, T. Kato, J. Liu, M. Takano, N. Kozai & S. Utsunomiya, *Environmental Science; Processes & Impacts*, 25 (7), 1204-1212 (2023).

Book

- 1) Current location of fuel debris chemistry, N. Sato, A. Kirishima, T. Sasaki, M. Takano, Y. Kumagai, S. Sato & K. Tanaka, Tohoku University Press, Sendai ISBN978-4-861633-390-4 (2023) (*in Japanese*).

Research Group for Nuclear Fuel Cycle Science

Papers

- 1) Efficient separation of americium by a mixed solvent of two extractants, a diamideamine and a nitrilotriacetamide, H. Suzuki & Y. Ban, *Anal. Sci.* 39, 1341 (2023).
- 2) Effect of decay heat on pyrochemical reprocessing of minor actinide transmutation nitride fuels, H. Hayashi, Y. Tsubata & T. Sato, *Trans. At. Energy Soc. Jpn.* 22(3), 97 (2023) (*in Japanese*).
- 3) A demonstration test to separate minor actinides in high-level liquid waste by N,N,N',N',N'',N''-hexaoctyl nitrilotriacetamide (HONTA) using mixer-settler extractors in a hot cell, Y. Ban, H. Suzuki, S. Hotoku & Y. Tsubata, *Solvent Extr. Res. Dev., Jpn.* 31(1), 1 (2024).
- 4) Extraction of Rh(III) from hydrochloric acid by protonated NTAamide(C6) and analogous compounds and understanding of extraction equilibria by using UV spectroscopy and DFT calculations, Y. Sasaki, M. Kaneko, Y. Ban, R. Kinoshita, M. Matsumiya, K. Shinoku & H. Shiroishi, *Anal. Sci.* 39(9), 1575 (2023).
- 5) CO9-1 Extraction chromatography and solvent extraction of Eu using TEHDGA, K. Otsu, M. Ikeno, C. Saiga, S. Takahashi, C. Kato, T. Matsumura, H. Suzuki, S. Fukutani & T. Fujii, *KURNS PROGRESS REPORT 2022*, 224 (2023).

Patent

- 1) H. Suzuki & T. Matsumura, "Extraction method of americium", Japanese Patent 7333057 (2023.08.16)

Chemistry, Environment, and Radiation Division

Research Group for Environmental Science

Papers

- 1) Soil dust and bioaerosols as potential sources for resuspended ^{137}Cs occurring near the Fukushima Dai-ichi nuclear power plant, M. Ota, S. Takahara, K. Yoshimura, A. Nagakubo, J. Hirouchi, N. Hayashi, T. Abe, H. Funaki & H. Nagai, *J. Environ. Radioact.* 264, 107198 (2023).
- 2) Tracking the behavior and characteristics of microplastics using a multi-analytical approach: a case study in two contrasting coastal areas of Japan, B. Battulga, M. Atarashi-Andoh, M. Matsueda & J. Koarashi, *Environ. Sci. Pollut. Res.* 30, 77226-77237 (2023).
- 3) Plastic-associated metal(loid)s in the urban river environments of Mongolia, B. Battulga, M. Atarashi-Andoh, J. Koarashi, B. Oyuntsetseg & M. Kawahigashi, *Ecotoxicol. Environ. Saf.* 261, 115100 (2023).
- 4) Effect of soil organic matter on the fate of ^{137}Cs vertical distribution in forest soils, J. Koarashi, M. Atarashi-Andoh & S. Nishimura, *Ecotoxicol. Environ. Saf.* 262, 115177 (2023).
- 5) Thirty-year prediction of ^{137}Cs supply from rivers to coastal waters off Fukushima considering human activities, T. Ikenoue, H. Shimadera, T. Nakanishi & A. Kondo, *Water* 15, 2734 (2023).
- 6) Shift in the rhizosphere microbial communities between growing- and low-temperature dormant seasons in a northern hardwood forest, M. Nakayama & R. Tatenno, *Plant Soil*, <https://doi.org/10.1007/s11104-023-06391-y> (2023).
- 7) Large-eddy simulation of plume dispersion in a turbulent boundary layer flow generated by a dynamically controlled recycling method, H. Nakayama & T. Takemi, *Atmos. Sci. Lett.* 25, e1204 (2024).
- 8) Behavior of radiocesium (^{137}Cs) on the coastal seafloor near the Fukushima Daiichi Nuclear Power Plant inferred from radiocesium distributions in long cores, T. Nakanishi, T. Tsuruta, T. Misonou, T. Shiribiki, Y. Urabe & Y. Sanada, *J. Coast. Res.* 116, 161-165 (2024).
- 9) Some considerations on the dependence to numerical schemes of Lagrangian radionuclide transport models for the aquatic environment, R. Periañez, I. Brovchenko, K. T. Jung, K. O. Kim, L. Liptak, A. Little, T. Kobayashi, V. Maderich, B. I. Min & K. S. Suh, *J. Environ. Radioact.* 261, 107138 (2023).
- 10) Factors regulating the concentration of particulate iodine in coastal seawater, Y. Satoh, S. Otsuka, T. Suzuki & T. Nakanishi, *Limnol. Oceanogr.* 68, 1580-1594 (2023).
- 11) Simulation study on ^3H behavior in the Fukushima coastal region: comparison of influences of discharges from the Fukushima Daiichi and rivers, K. Sakuma, S. Yamada, M. Machida, H. Kurikami, T. Misonou, T. Nakanishi & K. Iijima, *Mar. Pollut. Bull.* 192, 115054 (2023).
- 12) Stable C and N isotope abundances in water-extractable organic matter from air-dried soils as potential indices of microbially utilized organic matter, H. Nagano, M. Atarashi-Andoh, S. Tanaka, T. Yomogida, N. Kozai & J. Koarashi, *Front. For. Glob. Change* 6, 1228053 (2023).
- 13) Root endophytic bacterial and fungal communities in a natural hot desert are differentially regulated in dry and wet seasons by stochastic processes and functional traits, T. Taniguchi, K. Isobe, S. Imada, M. M. Eltayeb, Y. Akaji, M. Nakayama, M. F. Allen & E. L. Aronson, *Sci. Total Environ.* 899, 165524 (2023).
- 14) Sequential loss-on-ignition as a simple method for evaluating the stability of soil organic matter under actual environmental conditions, Y. Satoh, S. Ishizuka, S. Hiradate, M. Atarashi-Andoh, H. Nagano & J. Koarashi, *Environ. Res.* 239, 117224 (2023).
- 15) Front line of countermeasures against radiation terrorism in urban area (2); Development of LHADDAS and its application to countermeasures for radiological terrorism, H. Nakayama & D. Satoh, *J. At. Energy Soc. Jpn.* 65, 621-624 (2023) (in Japanese).

JAEA Report

- 1) Improvement of the resuspension model for OSCAAR using the atmosphere-soil-vegetation model SOLVEG-R (Contract Research), C.

Nakanishi, M. Ota, J. Hirouchi & S. Takahara, *JAEA-Research*, 2023-012 (2024) (in Japanese).

Book

- 1) 7.2 Source term, H. Terada, 気象研究ノート (Japanese).
(*Kisho-kenkyu note*) 248, 115-121 (2023) (in

Research Group for Radiation Transport Analysis

Papers

- 1) Nature of the physicochemical process in water photolysis uncovered by a computer simulation, T. Kai, T. Toigawa, M. Ukai, K. Fujii, R. Watanabe & A. Yokoya, *The Journal of chemical physics* 158(16) (2023).
- 2) A terrestrial SER estimation methodology based on simulation coupled with one-time neutron irradiation testing, S.-I. Abe, M. Hashimoto, W. Liao, T. Kato, H. Asai, K. Shimbo, H. Matsuyama, T. Sato, K. Kobayashi & Y. Watanabe, *IEEE Trans. Nucl. Sci.* 70(8), 1652 (2023).
- 3) Modelling oxygen effects on the in- and out-of-field radiosensitivity of cells exposed to intensity-modulated radiation fields, Y. Matsuya, S.J. McMahon, K.T. Butterworth, Y. Yachi, R. Saga, T. Sato & K.M. Prise, *Phys. Med. Biol.* 68(9), 095008 (2023).
- 4) Biophysical simulations for estimating biological effects after exposure to ionizing radiation: current state and future prospect, Y. Matsuya & R. Saga, *Radiat. Environ. Med.* 12(2), 81-90 (2023).
- 5) Improvement of the hybrid approach between Monte Carlo simulation and analytical function for calculating microdosimetric probability densities in macroscopic matter, T. Sato, Y. Matsuya, T. Ogawa, T. Kai, Y. Hirata, S. Tsuda & A. Parisi, *Phys. Med. Biol.* 68(15), 155005 (2023).
- 6) Development of nuclear de-excitation model EBITEM Ver.2, T. Ogawa, S. Hashimoto & T. Sato, *J. Nucl. Sci. Technol.*, 61, 68-73 (2024).
- 7) Isotopic composition of enriched ^{100}Mo for production of medical $^{99\text{m}}\text{Tc}$ by $^{100}\text{Mo}(p,2n)^{99\text{m}}\text{Tc}$, S. Hashimoto & Y. Nagai, *J. Phys. Soc. Jpn.* 92, 124202 (2023).
- 8) Development of an electron track-structure mode for arbitrary semiconductor materials in PHITS, Y. Hirata, T. Kai, T. Ogawa, Y. Matsuya & T. Sato, *Jpn. J. Appl. Phys.*, 62, 106001 (2023).
- 9) Recent improvements of the particle and heavy ion transport code system; PHITS version 3.33, T. Sato, Y. Iwamoto, S. Hashimoto, T. Ogawa, T. Furuta, S. Abe, T. Kai, Y. Matsuya, N. Matsuda, Y. Hirata, T. Sekikawa, L. Yao, P. E. Tsai, H. N. Hunter, H. Iwase, Y. Sakaki, K. Sugihara, N. Shigyo, L. Sihver & K. Niita, *J. Nucl. Sci. Technol.* 61, 127-135 (2024).
- 10) First-principles simulation of an ejected electron produced by monochromatic deposition energy to water at the femtosecond order, T. Kai, T. Toigawa, Y. Matsuya, Y. Hirata, T. Tezuka, H. Tsuchida & A. Yokoya, *RSC advances* 13(46) 32371-32380 (2023).
- 11) Development of a model for evaluating the luminescence intensity of phosphors based on the PHITS track-structure simulation, Y. Hirata, T. Kai, T. Ogawa, Y. Matsuya & T. Sato, *Nucl. Inst. Meth. B*, 547, 165183 (2024).
- 12) A step-by-step chemical code for estimating yields of free radicals based on electron track-structure mode in the PHITS code, Y. Matsuya, Y. Yoshii, T. Kusumoto, Y. Hirata, K. Akamatsu, T. Sato & T. Kai, *Phys. Med. Biol.* 69, 035005 (2024).
- 13) Changes in molecular conformation and electronic structure of DNA under ^{12}C ions based on first-principles calculations, T. Sekikawa, Y. Matsuya, B. Hwang, M. Ishizaka, H. Kawai, Y. Ono, T. Sato & T. Kai, *Nucl. Inst. Meth. B* 548, 165231 (2024).
- 14) Virtual photon approach of cathodoluminescence and ion-beam induced luminescence of solids, J-M. Constantini, T. Ogawa & D. Gourier, *J. Phys.: Condens. Matter* 35, 285701 (2023).
- 15) SUMRAY: R and Python codes for calculating cancer risk due to radiation exposure of a population, M. Sasaki, K. Furukawa, D. Satoh, K. Shimada, S.'i. Kudo, S. Takagi, S. Takahara & M. Kai, *J. Radiation Protection Res.* 48(2), 90 (2023).
- 16) Neutron production in the interaction of 200-MeV deuterons with Li, Be, C, Al, Cu, Nb, In, Ta, and Au, Y. Watanabe, H. Sadamatsu, S. Araki, K.

- Nakano, S. Kawase, T. Kin, Y. Iwamoto, D. Satoh, M. Hagiwara, H. Yashima, T. Shima & S. Nakayama, *EPJ Web of Conf.* 284, 01041 (2023).
- 17) Quantitative visualization of a radioactive plume with harmonizing gamma-ray imaging spectrometry and real-time atmospheric dispersion simulation based on 3D wind observation, H. Nagai, Y. Furuta, H. Nakayama & D. Satoh, *J. Nucl. Sci. Technol.* 60(11), 1345 (2023).
- 18) Neutron-production double-differential cross sections of ^{nat}Pb and ^{209}Bi in proton-induced reactions near 100 MeV, H. Iwamoto, S. Meigo, D. Satoh, Y. Iwamoto, Y. Ishi, T. Uesugi, H. Yashima, K. Nishio, K. Sugihara, Y. Çelik & A. Stankovskiy, *Nucl. Inst. Met. B* 544, 165107 (2023).
- 19) Development of DynamicMC for PHITS Monte Carlo package, H. Watabe, T. Sato, et al., *Radiation Protection Dosimetry*, 200(2), 130–142, <https://doi.org/10.1093/rpd/ncad278> (2024).
- 20) Modeling for predicting survival fraction of cells after ultra-high dose rate irradiation, Y. Shiraishi, Y. Matsuya, T. Kusumoto & H. Fukunaga, *Phys. Med. Biol.* 69 015017 (2023).
- 21) Atmospheric ionization profiles by solar X-rays, solar protons, and radiation belt electrons in September 2017 space weather event, K. Murase, R. Kataoka, T. Nishiyama, K. Sato, M. Tsutsumi, Y. Tanaka, Y. Ogawa & T. Sato, *Space Weather*, 21, e2023SW003651, <https://doi.org/10.1029/2023SW003651> (2023).
- 22) System of radiological protection; towards a consistent framework on earth and in space, W. Ruehm, N. Ban, J. Chen, M. Durante, S. El-Jaby, T. Komiyama, C. Li, O. Ozasa, T. Sato, et al., *Journal of Medical Physics* 34, 4-13 <https://doi.org/10.1016/j.zemedi.2024.01.004> (2024).
- 23) Comparison of dose and risk estimates between ISS partner agencies for a 30-day lunar mission, M. Shavers, E. Semones, V. Shurshakov, M. Dobynde, T. Sato, T. Komiyama, L. Tomi, J. Chen, S. El-Jaby, U. Straube, C. Li & W. Rühm, *Zeitschrift für Medizinische Physik*, 34(1) 31-43 (2024).
- 24) Soft errors in semiconductor devices due to environmental radiation -simulation of soft errors due to environmental radiations-, S. Abe, *J. At. Energy Soc. Jpn.* 65(5), 326 (2023) (*in Japanese*).
- 25) Report on the 2023 Nuclear Data Workshop, Y. Iwamoto, *Nuclear Data News* 137, 54-61 (2024) (*in Japanese*).
- 26) Simulation of cosmic ray induced soft errors using PHITS, S. Abe, *CROSS T&T* 76, 39-43 (2024) (*in Japanese*).

Research Group for Nuclear Chemistry

Papers

- 1) A Raman spectroscopy study of bicarbonate effects on UO_{2+x} , J. McGrady, Y. Kumagai, M. Watanabe, A. Kirishima, D. Akiyama, S. Kimuro & T. Ishidera, *J. Nucl. Sci. Technol.* 60(12), 1586 (2023).
- 2) UO_2 dissolution in bicarbonate solution with H_2O_2 ; the effect of temperature, J. McGrady, Y. Kumagai, Y. Kitatsuji, A. Kirishima, D. Akiyama & M. Watanabe, *RSC Adv.* 13(40), 28021 (2023).
- 3) Extraction of Rh(III) from hydrochloric acid by protonated NTAamide(C6) and analogous compounds and understanding of extraction equilibria by using UV spectroscopy and DFT calculations, Y. Sasaki, M. Kaneko, Y. Ban, R. Kinoshita, M. Matsumiya, K. Shinoku & H. Shiroishi, *Anal. Sci.* 39(9), 1575 (2023).
- 4) Uranium hydroxide/oxide deposits on uranyl reduction, K. Ouchi, D. Matsumura, T. Tsuji, T. Kobayashi, H. Otobe & Y. Kitatsuji, *RSC Adv.* 13(24), 16321 (2023).
- 5) Preliminary studies of XANES and DFT calculation of Ru extraction by imino-diacetamide and related compounds, Y. Sasaki, M. Nakase, M. Kaneko, T. Kobayashi, K. Takeshita & M. Matsumiya, *Anal. Sci.* 40, 335 (2024).
- 6) Free volume study of sulfonated FEP proton exchange membrane, T. Oka, A. Oshima & M. Washio, *Radiation Phys. Chem.*, 215, 111364 (2024).
- 7) Development of a quantification method for Zr isotopes in solid samples by LA-ICP-MS for rapid analysis of Zr-93 in high-level radioactive wastes, S. Morii, T. Yomogida, S. Asai, K. Ouchi, T. Oka & Y. Kitatsuji, *BUNSEKI KAGAKU* 72(10.11) 441(2023) (*in Japanese*).
- 8) Examination of a new quantification method of Zr isotopes in solid samples by LA-ICP-MS for Zr-93 analysis in difficult to dissolve radioactive wastes, S. Morii, T. Yomogida, S. Asai, K. Ouchi, T. Oka & Y. Kitatsuji, *Proc. the 24th Workshop on*

- Environmental Radioactivity, KEK Proceedings* 2023-2, 132(2023) (in Japanese).
- 9) Application of transition-edge sensors for micro-X-ray fluorescence measurements and micro-X-ray absorption near edge structure spectroscopy: a case study of uranium speciation in biotite obtained from a uranium mine, T. Yomogida, T. Hashimoto, T. Okumura, S. Yamada, H. Tatsuno, H. Noda, R. Hayakawa, S. Okada, S. Takatori, T. Isobe, T. Hiraki, T. Sato, Y. Toyama, Y. Ichinohe, O. Sekizawa, K. Nitta, Y. Kurihara, S. Fukushima, T. Uruga, Y. Kitatsuji & Y. Takahashi, *Analyst* 149(10) 2932 (2024).
- 10) Stable C and N isotope abundances in water-extractable organic matter from air-dried soils as potential indices of microbially utilized organic matter, H. Nagano, M. Atarashi-Andoh, S. Tanaka, T. Yomogida, N. Kozai & J. Koarashi, *Frontiers Forests Global Change* 6, 1228053 (2023).
- 11) Evaluation of the production amount of Ac-225 and its uncertainty through the $^{226}\text{Ra}(n,2n)$ reaction in the experimental fast reactor Joyo, Y. Sasaki, A. Sano, S. Sasaki, N. Iwamoto, K. Ouchi, Y. Kitatsuji, N. Takaki & S. Maeda, *J. Nucl. Sci. Technol.* 61(4), 509 (2024).
- 12) Formation of nanoscale protrusions on polymer films after atomic oxygen exposure: observations with positron annihilation lifetime spectroscopy, A. Goto, K. Michishio, T. Oka, M. Tagawa & S. Yamashita, *Langmuir* 39(34) 11954 (2023).
- 13) Radiation-induced dissolution of uranium oxide materials in water, Y. Kumagai, *Housyassenkagaku* 115, 43 (2023) (in Japanese).
- 14) Application of vibrational sum frequency generation spectroscopy to studies of chemical reactions on water surface and actinide interface chemistry, R. Kusaka, *Bunkou kenkyu* 72(4), 155 (2023) (in Japanese).
- 15) Studies on complex reactions of actinides in solution and development of analytical methods for small amounts of samples, K. Ouchi, *housyakagaku* 49, 3 (2024) (in Japanese).

Nuclear Science and Engineering Center

Paper

- 1) Quantitative visualization of a radioactive plume with harmonizing gamma-ray imaging spectrometry and real-time atmospheric dispersion simulation based on 3D wind observation, H. Nagai, Y. Furuta, H. Nakayama & D. Satoh, *J. Nucl. Sci. Technol.* 60(11), 1345 (2023).

Book

- 1) I. Prediction system for radioactive impacts in nuclear emergency (SPEEDI, WSPEEDI), H. Nagai & M. Chino, *気象研究ノート (Kisho-kenkyu note)* 248, 1 (2023) (in Japanese).

Reviewers

ISHIKAWA Norito, KAWAMURA Hideyuki, KUMAGAI Yuta,
KUSAKA Ryoji, NAKANISHI Takahiro, OKA Toshitaka,
ROVIRA Gerard, SUZUKI Takashi, TERADA Hiroaki,
TSUDA Shuichi

Editorial Board

- Chief Editor:

HAYASHI Hirokazu

- Editors:

ROVIRA Gerard, ISHIKAWA Norito, ABE Shin-ichiro,
KATO Chiaki, NAKAHARA Yukio

Nuclear Science and Engineering Center (NSEC)
Japan Atomic Energy Agency (JAEA)

2-4 Shirakata, Tokai-mura, Naka-gun, Ibaraki
319-1195. Japan

E-mail : nsec-web@jaea.go.jp

U R L : <https://nsec.jaea.go.jp/>